12-16-2014

Multivariate Remote Process Sensing for Online Quality Control of Injection Molding

Xinyao Tang
University of Connecticut - Storrs, xinyao.tang@uconn.edu

Multivariate Remote Process Sensing for Online Quality Control of Injection Molding

Xinyao Tang

B.S., Qingdao Technological University, 2012

A Thesis

Submitted in Partial Fulfillment of the

Requirements for the Degree of

Master of Science

At the

University of Connecticut

2015

APPROVAL PAGE

Masters of Science Thesis

Multivariate Remote Process Sensing for Online Quality Control of Injection Molding

Presented by

Xinyao Tang, B.S.

Major Advisor_____
Robert X. Gao

Associate Advisor_____
Jiong Tang

Associate Advisor_____
Chengyu Cao

University of Connecticut

2015

ACKNOWLEDGMENTS

My completion of M.S. degree could not have been accomplished without the countless critical and constructive input, suggestions, and supports from many people, and thereby it is my great pleasure to thank them for their continued help, encouragement, and contributions.

I would like to express my sincere gratitude to my M.S. advisor, Dr. Robert Gao, for his continuous support, patient guidance and insightful advise throughout my M.S. study. His persistence, enthusiasm, inspiration, and dedication to science have not only guided me to go through the hardships all the way to the achievements but also showed me how to conduct scientific research. I really appreciate that the training I received under his guidance, which, I believe, will great benefit my future career and life.

My special thanks are to my committee members, Dr. Jiong Tang and Dr. Chengyu Cao, for their great support, valued suggestions and continued encouragements. I offer my sincere appreciation for the guidance provided by my committee.

I also would like to thank to my collaborators: Dr. David Kazmer and Guthrie Gordon from University of Massachusetts, Lowell, for their help and support with experiment setup, professional machine operation, data collection and signal processing; and current and former Electromechanical Systems (EMS) Lab members: Dr. Zhaoyan Fan, Dr. Jinjiang Wang, Peng Wang, Xiyue Zou, Donald Karg, Fangfei Ju, and Yuji Tomizawa, for their friendship, support, encouragement, discussions and assistance.

I'd also like to gratefully acknowledge the funding provided to this research by the National Science Foundation under Grand No. CMMI-1000816/1000551.

Last and most importantly, to my caring, loving, and supportive wife, Zhao Zhao: my deepest gratitude for her great help, encouragement and support that accompanying me on the way to my obtaining the M.S. Degree. My heartfelt thanks.

TABLE OF CONTENTS

ABSTRACT

Multivariate Remote Process Sensing for Online Quality Control of Injection Molding

DECEMBER 2014

XINYAO TANG

B.S., QINGDAO TECHNOLOGICAL UNIVERSITY, CHINA

Directed by:

Professor Robert X. Gao

A new wireless multivariate sensor (MVS) is designed, prototyped, structurally embedded into a mold structure to provide in situ feedback of four process states within mold cavity: melt temperature, melt pressure, melt velocity and melt viscosity, which closely correlate to the quality of manufactured products through the constitutive viscoelastic behavior of the polymer being processed. The developed MVS enables the improved observability of injection molding and provides a new process instrumentation and control methodology that sets up, assures, and optimizes the quality of injected products. Relationship between the key in-process states and quality characteristics (e.g., thickness and width of the part) are established by incorporating governing physics for pressure-volume-temperature with other mechanistic models.

Detailed design of wireless multivariate sensing system is introduced in Chapter 2. The MVS for intelligent polymer processing incorporates a piezoelectric ring to acquire melt pressure, a thermopile to obtain melt temperature and a thermistor to achieve mold temperature. Chapter 3 investigates the mechanistic models that are derived to estimate melt velocity and melt viscosity. To enable the wireless data transmission through an enclosed metallic environment, which is a prevalent phenomenon in

manufacturing machinery, a coded-acoustic wave modulation scheme is proposed for multi-parameter transmission through an acoustic transmitter in Chapter 4. Signal attenuation and data loss due to wave diffraction and refection was theoretically and experimentally studied on the models of representative machine structures: rectangular and angled structures, where the effect of carrier wav frequency and placement of receiver and transmitter was also investigated experimentally. The presented acoustic wireless sensing method can be applied to a wide range of processing monitoring scenarios.

To obtain the desired critical-to-quality attributes (CTQs) of precision manufactured products, process and instrumentation must be consciously designed such that the key process variables (KPVs) are observable and controllable. A support vector regression (SVR) model has been developed in Chapter 5 to relate the MVS-sensor outputs, which are obtained during the injection molding process, to the part dimensions, which are measured off-line, for establishing a correlation that serves as the basis for online part quality estimation and future production prediction. The proposed quality control system with a high accuracy of 3 errors per million opportunities as specified by six sigma methodologies can ultimately enable fully automatic, high quality production.

A framework of orthogonality analysis based on principle component analysis is established in Chapter 6 for quantification of sensory data correlation, which provides a systematic explanation on why a multivariate sensor that quantifies four parameters within the same package has consistently outperformed multiple single-parameter sensors, under various operation conditions, thereby contributing to the theory of data fusion for measurement enhancement.

Keywords: multivariate sensing; in-process monitoring; acoustic wave; wireless transmission; online quality control;

LIST OF TABLES

LIST OF FIGURES

CHAPTER 1

INTRODUCTION

1.1 Objective

The objective of this research project is to improve observability of injection molding and characterize its relationship with product quality and manufacturing productivity in polymer processing. A new wireless multivariate sensor is investigated, developed and prototyped to provide online feedback of four key process states critical to injected product quality: melt pressure, melt temperature, melt velocity, and melt viscosity measured within the mold cavity. This research, enabled by such a new multivariate sensing method, leads to a new process instrumentation and quality control methodology that assures and optimizes the quality of injection molded parts.

1.2 Background of Research

Polymer processing enables mass production of a variety of complex products at low cost. In these processes, thermoplastic feedstock in the form of pellets is melted through conduction and viscous dissipation to form a homogeneous melt [1]. Once a melt is collected, it is forced through a die or into a mold to form an extruded profile or other complex shape. Prior to the 1970s, the majority of plastics molding machines utilized open-loop control for most subsystems. Since the advent of programmable logic control, the majority of process conditions have become individually controlled via single-input single-output PID algorithms [2]. Continuing advances in machine and control system designs have been made such that response and repeatability of the machinery have improved dramatically [3, 4]. While such advances in machine control are important, the polymer states within the mold ultimately determine the molded product quality [5]. However, no single control strategy or system design has been universally successful and defective components are continuing to be manufactured in high volume production [6].

Control of polymer processing is impeded by the transient and distributed state of the polymer melt. Every plastics manufacturing application is unique with respect to the mold geometry, material properties, and processing conditions. The ideal sensor suite is therefore unique with respect to the number, type, position, and use of signals to provide the best process observability at lowest cost. Four key states – pressure, temperature, velocity, and viscosity – are known to govern the quality of manufactured products through the constitutive viscoelastic behavior of the polymer being processed [7, 8]. Yet, the vast majority of production machinery uses conventional machine sensors for closed-loop control. For example, plastics manufacturers typically use sensors and set control limits assuming linear models that are hopefully "good enough." As a result, the *in-situ* states of the polymer are neither accurately observed nor properly controlled, leading to suboptimal processes, low yields, and environmental waste [9].

A conventional, closed-loop injection molding machine with varying levels of feedback is illustrated in Fig. 1. It has been widely acknowledged that obtaining state feedback about the process at many places within the mold cavity is advantageous [10-13]. Because the mold usually contains fairly complicated geometry (including cooling lines, side cores, and ejector pins), it is very expensive to run additional wires through the mold to connect a sensor. As the number of sensors becomes large, the costs of "hardwiring" those sensors become prohibitive. This leads to a real limit of the number of sensors that can be placed inside an injection mold, and thus a limit on the amount of information that can be obtained about the injection molding process. It is clear that in many manufacturing processes today, ***retrieving*** the information is the bottleneck of controlling that process. Because of this limitation, current molding controller technology relies on machine and other cabled sensors for monitoring clamp force, barrel temperature, motor toque, screw position, nozzle pressure, and others [14-18]. While somewhat effective for process control, these sensors are in fact poor estimators of the manufactured part quality [19].

Striving to remain competitive and economically viable, domestic manufacturers are increasingly relying on fully automated systems for fault diagnosis, quality control, and materials handling [20]. Such system designs must operate in an on-line, in-process fashion for effective polymer process control and

optimization. Accordingly, there is an urgent need for more advanced and intelligent in-mold sensors that can provide comprehensive, real-time state feedback of the process internal to the mold where the product is formed. The measurement and retrieval of a complete set of process states remains one of the most significant barriers to the success of more advanced process control systems.

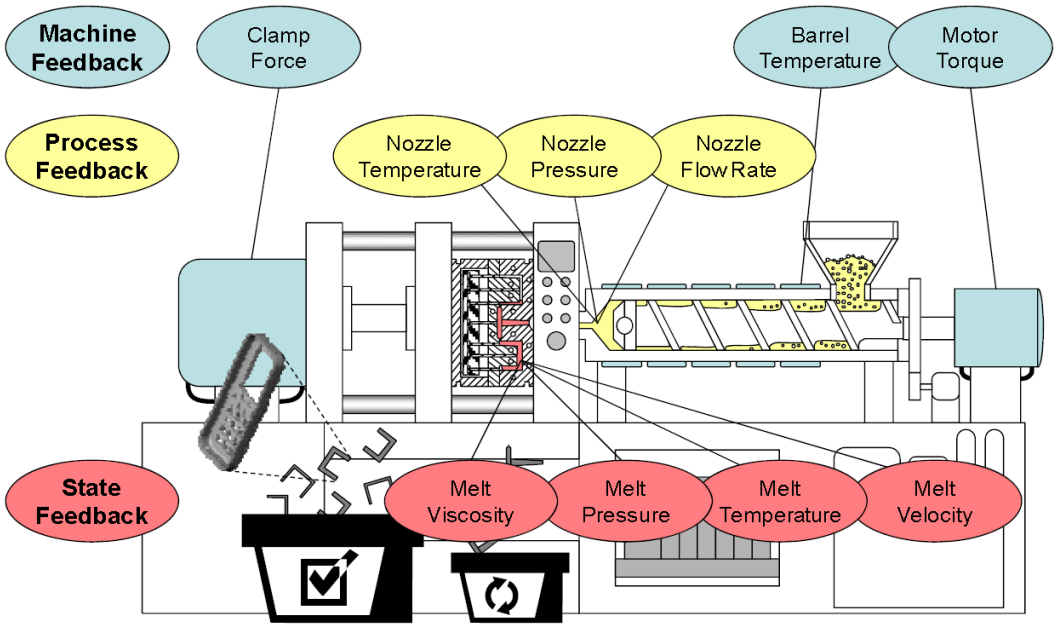

Figure 1-2: Feedback control system for injection molding

Many sensor systems have approached the remote sensing problem by utilizing active energy sensors such as sonar imaging or X-ray imaging [21-23]. This approach works well for biological systems where the material interfaces are well defined such as soft tissue and bone. However, when dealing with the interference of mold steel and the varying electromagnetic and acoustic properties of various kinds of polymers and fillers, these sensing techniques provide little usable process information. Previous research has investigated the use of acoustics for melt characterization [24, 25]. These sensors rely on the transmission and reflection of ultrasonic waves through the mold and polymer material. Although acoustic waves reflected by the polymer-mold interface provide a non-destructive means to monitor the bulk movement of the polymer melt, the melt pressure and temperature could not be resolved from the signals. The underlying issue is that the speed of sound is a function of the melt modulus and density, both of which

are in turn confounded with the temperature and pressure. Therefore, the approach is dependent on the local geometry of the mold, cooling lines, material properties, and processing conditions so that validation is required on an application-specific basis. Prior NSF-funded research [26-28] has led to the realization of a dual-parameter sensing method for monitoring the polymer melt directly within the mold cavity. Specifically, the sensor is embedded within the injection mold and acoustic waves were used to transmit measured signals to an external receiver outside of the mold, where no space limitation is present. The dual sensing method [29] was realized by exploring the thermal effect on dielectricity in the design of temperature sensor and temperature modulator, as shown in Fig. 1-3. The sensor harvests energy from the melt pressure change by means of a stack of piezo-ceramic rings. Besides serving as the energy source for the on-board electronics, the electrical charges generated also provided a direct measure for the molding pressure. By means of a threshold modulator, the charges are converted into voltage pulses. The sensor integrates a temperature-sensitive oscillator module (TSO) to convert the change of temperature into a shift in the carrier frequency of the ultrasonic pulses through a temperature sensitive capacitor. Thus, the melt pressure and temperature are respectively differentiated by the variation of two parameters related to the ultrasonic pulses: the number of the pulses and their carrier frequency. Research on energy harvesting [26-29], modulator design [31, 32], and acoustic pulse propagation have enabled the prototyping and experimental evaluation of a wireless dual-parameter sensor in an injection molding process. Comparison with commercially available, wired pressure and temperature sensors demonstrates that pressure and temperature data measured by the dual-parameter sensor well match those from the commercial sensors in terms of capturing the process dynamics. As shown in Fig. 1-4, key transitions between different molding stages were accurately captured by the dual-parameter sensor. For example, between approximately 0.6~0.8 sec, a linear increase of the melt pressure is identified (Fig. 1-4a), indicating that polymer melt was injected into the mold cavity at a constant velocity, until the mold is filled. Successful measurement of the mold temperature was also observed as shown in Fig. 1-4b.

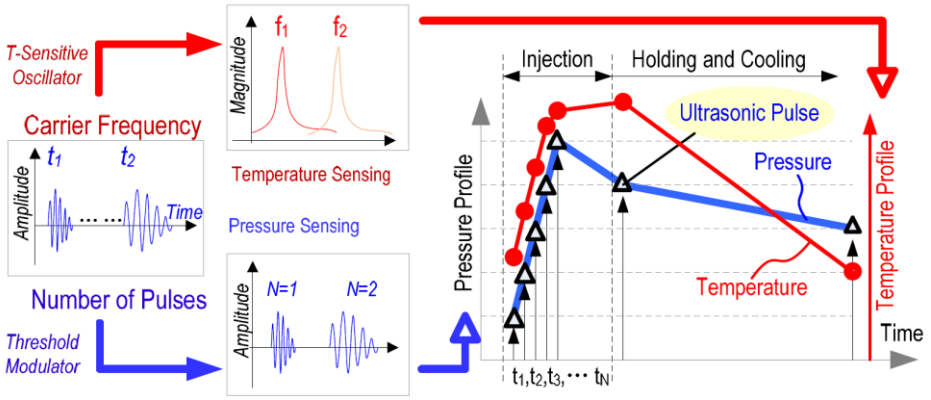

Figure 1-3: Working principle of the dual-parameter sensor

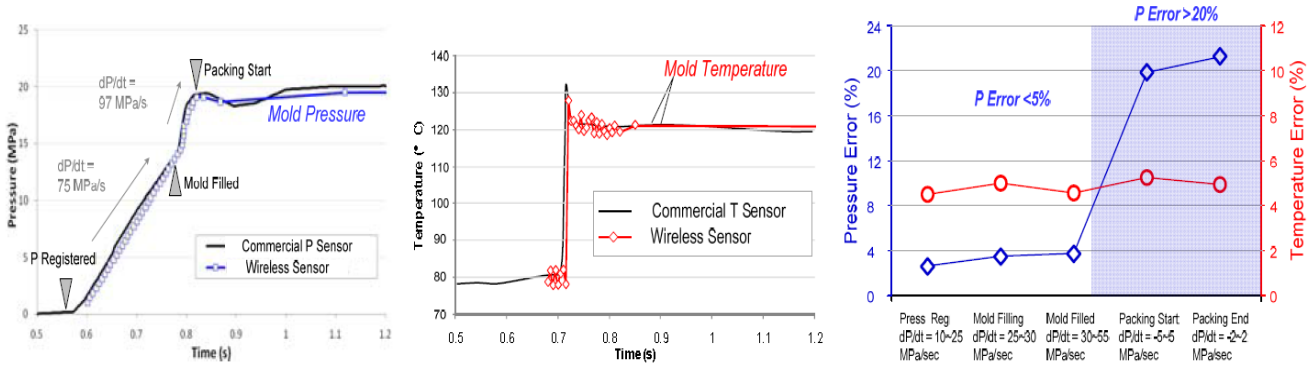

(a) pressure (b) temperature (c) measurement error

Figure 1-4: Pressure and temperature retrieved in real-time, during injection molding process

1.3 Problem Statement and Research Directions

The fundamental difficulty in polymer process control is the indeterminate and distributed nature of the polymer throughout the mold. As such, recent control developments have rightly focused on closing the loop between the machine parameters and the polymer state. For example, closed-loop control of cavity pressure could automatically compensate for variations in melt viscosity and injection pressure to achieve a consistent process and uniform set of product attributes [32]. Mann introduced one of the first pressure control schemes by using modulated pressure relief valves [33], and Abu Fara developed a process control model by relating the cavity pressure response to open-loop perturbations [34]. Srinivasan later used these models to propose a learning controller for closed-loop cavity pressure control [35]. Adaptive control

methods have also been proposed to track cavity pressure profile at usually one location in the mold [35]. Dynamic melt flow regulators have also been developed to allow independent, real-time control of the melt flow and pressure at multiple points in the mold [36-40]. More recently, Turng integrated weight feedback into a cascade closed loop control [41]. Yet, these machine and control system designs remain limited by the lack of observability of the process states.

It should not be surprising that as more process states are obtained, the observability of the process is improved. The results [42] shown in Fig. 1-1 indicate that 92.5% of the part quality (measured here as length of a tensile bar specimen) can be explained by retrieving and analyzing information on four process parameters: melt pressure, melt temperature, melt velocity, and melt viscosity. Further improvement of up to 95.7% can be expected if the mold temperature can be included. Our prior NSF research investigating the use of this process data with real time, on-line simulations [43, 44] indicates that this level of observability can be sufficient for automated process and quality control but must be validated for the application requirements. Further analysis of alternative sensor streams indicated that the process states derived from the in-mold sensors [45] were consistently preferred over the machine states with respect to predicting the influence in the molded part quality. These results suggest that future research should investigate the feasibility of retrieving *multiple* process states from a *single* in-mold sensor with the concurrent development of optimal instrumentation methodologies.

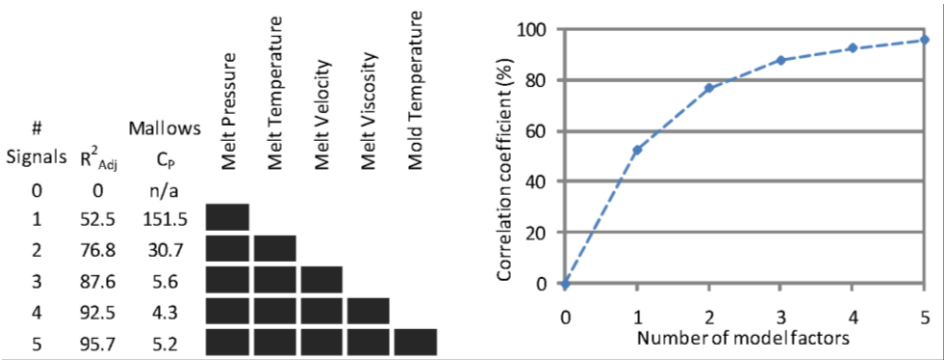

Figure 1-1: Improved observability with additional signals

The proposed sensor is self-energized through energy harvested from a stack of piezoelectric (PZT) rings that extracts energy from the pressure differentials in the molding process. Previous analyses and validated designs [46, 47] indicate that an average power of ~ 200 mW can be extracted given typical pressure dynamic per 1 cm^3 of PZT volume. Compared to the previous designs, however, there are four significant challenges to be met: 1) determination of the melt velocity by means of infrared based temperature sensing, 2) inference of melt viscosity based on the melt velocity and pressure differential, 3) encoding of acoustic waves for wirelessly transmitting multiple process state parameters from a single acoustic pulse train, and 4) online optimization of the quality of injection molded parts using support vector regression to establish the non-linear relationship between processing states and product characteristics.

1.4 Thesis Outline

This thesis is organized as following:

- Chapter 2 presents the hardware design and mechanical packaging of a wireless embedded multivariate sensing system for online measurements of polymer processing states, including melt pressure, temperature, velocity and viscosity.
- Chapter 3 investigates the performance evaluation of the designed wireless multivariate sensor (MVS) both through the simulation and experimental analysis. Reference of melt velocity by means of infrared based temperature sensing and melt viscosity based on the melt velocity and pressure differential is studied as well to further validate the reliability and accuracy of the MVS measurements.
- Chapter 4 proposes an acoustic based wireless signal transmission through the metallic shielding for multiple state parameters transmission during injection molding process monitoring. A quantitative analysis of factors affecting the performance of signal transmission using acoustic wave including frequency, bandwidth, signal-to-noise ratio, data bit-rate, etc. Signal attenuation and data loss due to wave diffraction and reflections is first numerically studies using finite element models of representative machine structures. Experimental

evaluation of these models with operating production machinery quantifies the accuracy and reliability of in situ acoustic signal transmission methods for precision metrology in manufacturing.

- Chapter 5 presents the non-linear relationship between the four key in-process states within the injection cavity, including melt temperature, melt pressure, melt velocity, and melt viscosity, and quality characteristic (e.g., thickness and width of the part) of the injection molded parts by incorporating governing physics for pressure-volume-temperature with support vector regression methods. Good agreement between sensor measurements and experimental results is confirmed from tests performed on a production-grade machine.
- Chapter 6 summarizes both theoretical and experimental contributions of this dissertation, discusses broader impact and potential applications, and outlines some future research directions based on the presented research.

CHAPTER 2

DESIGN OF WIRELESS MULTIVARIATE SENSING SYSTEM

2.1 Overview

Polymer process enables mass production of a variety of complex yet economical products. While control of polymer processing is impeded by the transient and distributed state of the polymer melt. Every plastics manufacturing application is unique with respect to the mold geometry, material properties, and processing conditions. Four key states – pressure, temperature, velocity, and viscosity – are known to govern the quality of manufactured products through the constitutive viscoelastic behavior of the polymer being processed [7, 8]. Yet, the vast majority of production machinery uses conventional machine sensors for closed-loop control. For example, plastics manufacturers typically use sensors and set control limits assuming linear models that are hopefully "good enough." As a result, the *in-situ* states of the polymer are neither accurately observed nor properly controlled, leading to suboptimal processes, low yields, and environmental waste [9].

A conventional, closed-loop injection molding machine with varying levels of feedback is illustrated in Fig. 1. It has been widely acknowledged that obtaining state feedback about the process at many places within the mold cavity is advantageous [10-13]. Because the mold usually contains fairly complicated geometry (including cooling lines, side cores, and ejector pins), it is very expensive to run additional wires through the mold to connect a sensor. As the number of sensors becomes large, the costs of "hardwiring" those sensors become prohibitive. This leads to a real limit of the number of sensors that can be placed inside an injection mold, and thus a limit on the amount of information that can be obtained about the injection molding process. It is clear that in many manufacturing processes today, ***retrieving*** the information is the bottleneck of controlling that process. Because of this limitation, current molding controller technology relies on machine and other cabled sensors for monitoring clamp force, barrel temperature,

motor toque, screw position, nozzle pressure, and others [14-18]. While somewhat effective for process control, these sensors are in fact poor estimators of the manufactured part quality [19].

Striving to remain competitive and economically viable, domestic manufacturers are increasingly relying on fully automated systems for fault diagnosis, quality control, and materials handling. Such system designs must operate in an on-line, in-process fashion for effective polymer process control and optimization. Accordingly, a wireless embedded multivariate sensing system is urgently needed, which can provide comprehensive, real-time sate feedback of the process internal to the mold where the product is formed.

2.2 Mechatronic Design Philosophy

2.2.1 Melt pressure

The melt pressure is sensed by acquisition of charge accumulated through the piezoelectric effect from the imposed stress on the PZT ring. For a melt pressure, P, impinging on a lens radius, R, the static output voltage can be expressed as:

$$V = \frac{g_{33} \cdot P \cdot H \cdot R^2}{(OD^2 - ID^2)/4} \tag{2-1}$$

where g_{33} is a voltage constant, *H* is the ring thickness, *OD* and *ID* are the outside and inside diameter respectively. For example, the design with *H* equals to 1 mm and a voltage constant of 25.4 Vm/N, the voltage sensitivity will be 8.47 V/MPa. The maximum pressure is constrained by the maximum stress that can be applied to the zinc selenide lens, τ_{max}, which can be determined using the following equation, where *r* and *h* are the radius and thickness of the lens respectively:

$$\tau = P \cdot \frac{\pi R^2}{\pi r h} < \tau_{max} \tag{2-2}$$

where *r* and *h* are the radius and thickness of the lens at the location having the minimum cross-sectional area. In this design, the maximum shear stress on the lens will occur at the transition in the stepped thickness where *r* and R are 1.5 mm and h is 2 mm.

2.2.2 Melt temperature

The thermopile operates by measuring the incidence of radiation from the heated polymer melt. The thermal radiation, *Q*, is related to the fourth power of the temperature, according to the Stefan-Boltzmann law, *T*, the constant of proportionality σ (the Stefan-Boltzmann constant equal to 5.67·10-8 Wm−2K−4), and the emissivity ε of the object as [48]:

$$Q = \varepsilon \cdot \sigma \cdot T^4 \tag{2-3}$$

With respect to the thermopile, the output voltage, U, is also dependent on the ambient temperature, which we can assume is very close to the mold temperature, T_{mold}:

$$U = k \cdot \varepsilon \cdot (T^n - T_{mold}^n) \tag{2-4}$$

where *k* is the gain related to the detector, and n is dependent on the filter and sensor characteristics (n equals 4 for a perfect "black" characteristic and unlimited wavelength range). The temperature contains a thermistor to provide the compensation of ambient temperature, which could also provide the measurement of the mold temperature, capturing the temperature during the injection molding process.

2.2.3 Melt velocity

Advancements in IR detectors have led to fast response time (1 to 10^{-2}μs), making it possible to capture the temporal variation of the fast-changing temperature profile during the injection stage of a molding cycle where the melt front is flowing over the surface of the ZnSe lens, as illustrated in Fig. 2-1(a). The data in Fig. 2-1(b), acquired with a commercial in-mold pyrometer in our prior research, indicates that the rise time of the melt temperature is correlated with the melt velocity. The reason for the varying rise times is that the advancing melt front is traveling relatively slowly over the lens in comparison with the sampling rate, such that the infrared sensor is being excited by only the area of the polymer melt covering the sensor lens. Accordingly, a sensing method can be devised that exploits the functionality of the IR detector to provide for melt front velocity measurement. The relationship between the output of the IR sensor and the melt front velocity. As illustrated in Fig. 2-2 (b), temperature variation can be expressed as a function of the melt front location *x* and melt velocity v_x:

$$\frac{dT}{dt} = \frac{2r}{\pi r^2} \cdot T_0 \sqrt{1 - (1 - \frac{x}{r})^2} \cdot v_x \tag{2-5}$$

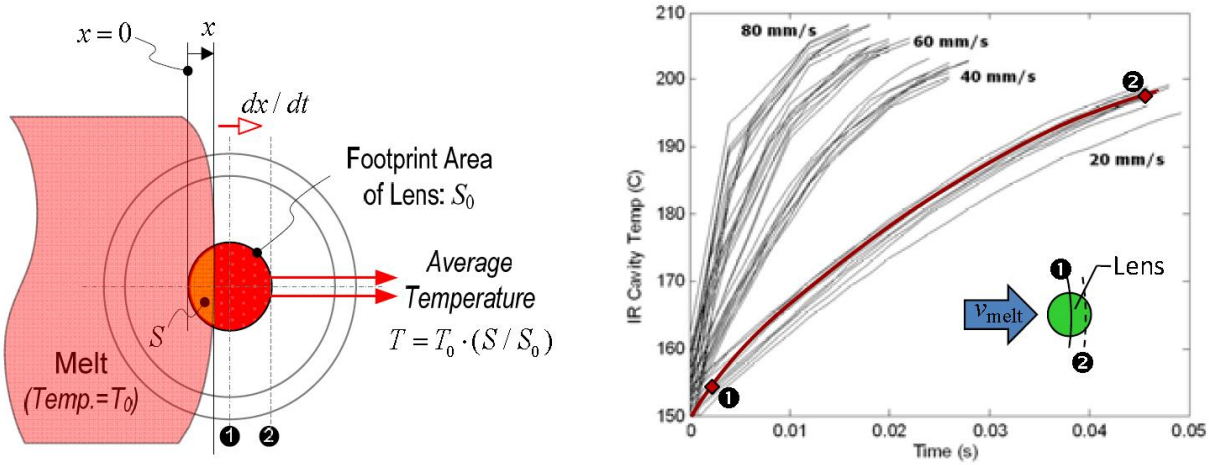

(a) Melt flowing over IR lens (b) Polymer states

Figure 2-1: Velocity sensing using the infrared detector

as the maximum temperature slope of the measured temperature curve occurs when the melt front crosses the centerline of the lens, where x=r. The velocity can be expressed as:

$$x = r \rightarrow v_x = \frac{\pi r^2}{T_0 \cdot 2r} \cdot \left(\frac{dT}{dt}\right)_{max} \tag{2-6}$$

Equation (2-6) indicates that the maximum temperature ramp can be approximated as a linear function of the melt velocity, while the coefficient can be determined from the designed or measured parameters S_0, r, and T_0. Hence, if the sampling rate for the infrared detector is sufficient to capture the maximum ramp rate of the melt temperature, the melt front velocity can be determined analytically.

2.2.4 Melt viscosity

Given the measured melt velocity and melt pressure, the melt viscosity, μ, can be accurately inferred based on its definition [49]:

$$\frac{dP}{dx} = \frac{12\mu v_x}{H^2} \rightarrow \mu = \frac{H^2}{12v_x}\frac{dP}{dx} \tag{2.9}$$

where H is the known thickness of the mold cavity, and v and dP/dt are the melt velocity and pressure, acquired by the multivariate sensor when the melt flow crosses the middle of the sensor. Some preliminary results from our previous research are shown in Fig. 2-2, for a spectrum of melt temperatures and velocities corresponding to Fig. 2-1. These results well match the expected rheological behavior of the polymer including a) shear thinning behavior causing a reduction in the viscosity at increasing melt velocities, and b) non-isothermal behavior providing a decrease in the melt viscosity at increasing melt temperatures.

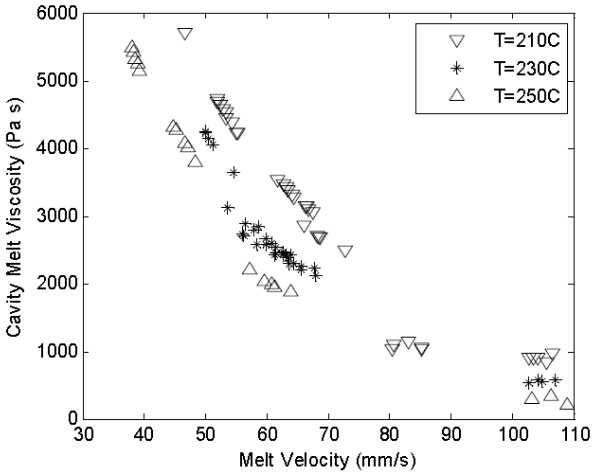

Figure 2-2: Viscosity data from previous research

2.3 Hardware Design

2.3.1 Electronic design

Based on literature survey and feedback from experts on polymer processing, the following requirements are to be satisfied by the multivariate sensing system:

1) Easy to install and battery recharging.
2) Minimal marker print on the final product.
3) Acoustic-based multiple signals transmission.
4) Adjustable data transmission rate and carrier wave frequencies.

5) Continuous operate for more than 3 hours.

6) Melt temperature, pressure, velocity, viscosity sensing

Since the multiple parameters and constraints are present that can influence the final outcome of the MVS design (e.g. the degree of functionality to be integrated into the device affects the device's dimension, and the same circuit complexity can be satisfied using different form factors, which could affect the power efficiency), a multi-disciplinary, concurrent design approach must be taken to ensure satisfactory fulfillment of the design objectives. This is addressed in the present study by established a need-metric matrix [50], as illustrated in Table 2-1. The need-metric matrix establishes a correlation between the global design needs and quantifiable design specifications to guide the concrete system design. As an example, the need for easy installation and recharging is identified as related to the manufacturing precision, packing dimensions, PCB dimensions, and material for packer, an indicated the dots in the corresponding metric columns.

Table 2-1: Need-Metric Matrix for the MVS

Needs \ **Metric**	Manufacturing precision	Package dimensions (L × D1)	PCB board dimensions (D2)	Sampling rate	Supply current	Power consumption	Robustness	Accuracy of measurements	Material for packer
Easy installation and recharging	•	•	•						•
Minimal marker print	•	•							•
Enable wireless data transmission				•	•	•	•		
System operation > 3 hours					•	•	•		
Adjustable data transmission rate								•	•
Multivariate sensing						•	•	•	

Given by the need-metric matrix, an embedded multivariate sensor that employs microprocessor and has the capability of signal sensing, data acquisition, wireless transmission, signal processing, etc., is needed. Therefore, the proposed system is designed to include basic elements: 1) a sensing interface to measure melt temperature, melt pressure, and mold temperature; 2) a central processing unit (CPU) for data acquisition, processing, etc.; 3) multiple parameter modulation unit for wireless data transmission; 4) a power management unit for energy-efficient operation.

In this study, the proposed MVS takes sensor measurements of melt pressure, melt temperature, mold temperature of the melt polymer during the injection molding process and inference melt velocity and melt viscosity through the microprocessor's further signal processing. A schematic sketch of the sensory components in the MVS is shown in Figure 2-3. Two sensors and one rechargeable battery are integrated in the system: 1) one temperature sensor (HMS Z 11GmbH, Dresden, Germany) placed behind the ZnSe lens, senses the melt temperature and transient temperature change of the polymer flowing across the lens; 2) one piezoelectric sensor (APC-841, Mackeyville, PA) installed behind the stand-off, measure the expansion and contraction behavior of the melt polymer crossing the lens; 3) one rechargeable li-ion button-sized battery embedded in the sensor package, provides the power supply for the PCB operation.

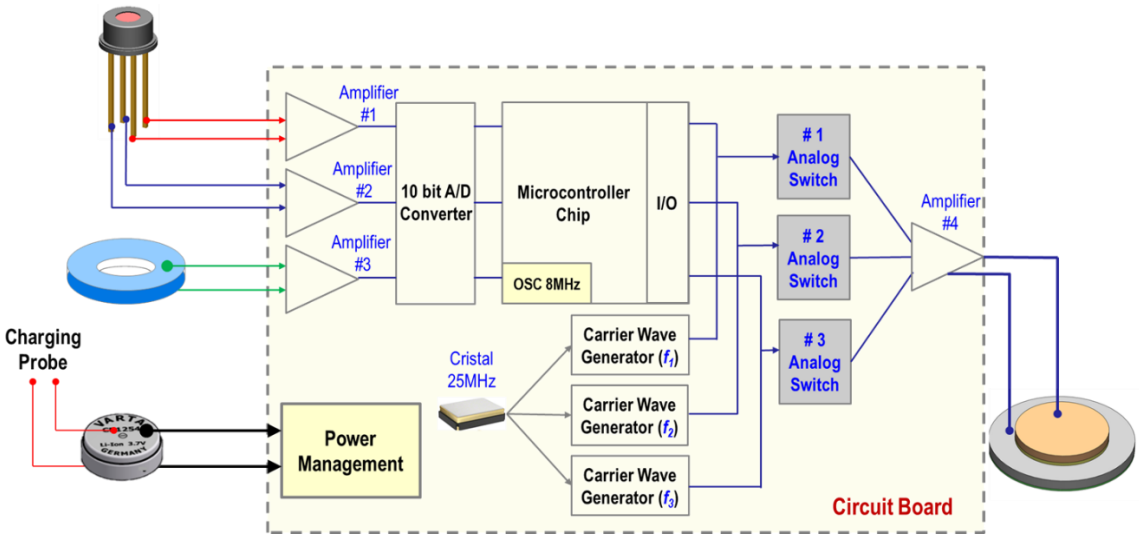

Figure 2-3: Circuit scheme of multivariate sensing system

Figure 2-3 shows the circuit scheme of multivariate sensor. The interface circuit is realized and performed by a charger amplifier and two feasible gained amplifiers. The system software acquires all the sensor signals via the on-chip 10 bit analog-to-digital converter (ADC) before sending to microcontroller (MCU) for signal processing. The functionality and primary operation of the MVS are controlled and conducted by the MCU. An amplitude modulation unit constitutes of three programmable carrier wave generator for multi-parameter modulation. An acoustic transmitter designed and prototyped according to the special wave frequencies is used for signal transmission. A rechargeable li-ion button sized battery and associated charging circuitry are employed for enabling long-term operation. The output of the battery is modulated by a voltage regulator to provide a 3.0-V supply voltage for the MVS. Figure 2-4 illustrates the PCB layout for the MVS, which is made up of four layers: 1) top signal layer; 2) inner GND layer; 3) inner +3 V layer; and 4) bottom signal layer. Specifically, the total size is 15 mm in diameter with two small outreaching ends for support and installation.

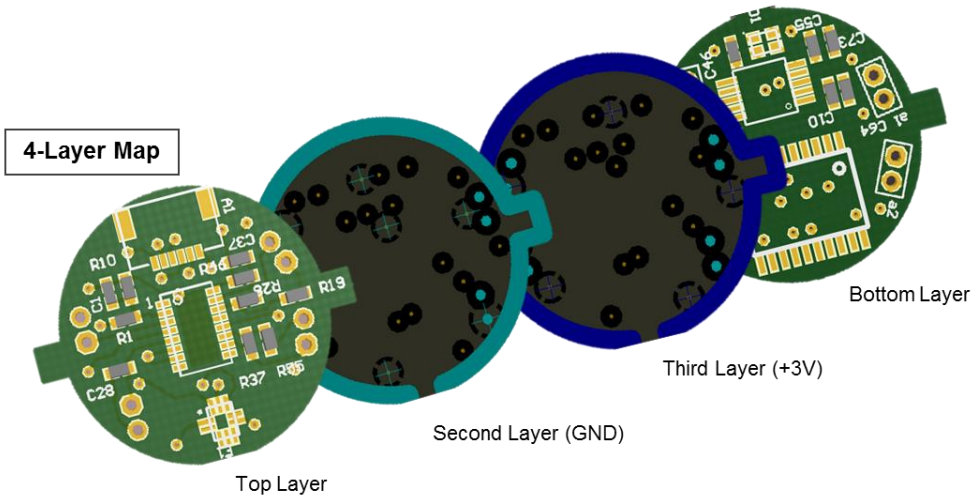

Figure 2-4: PCB layout map for multivariate sensing system

2.3.2 Mechanical packing

Figure 2-5 illustrates the details of mechanical packing for MVS. The material for lens are selected according to the temperature range during the polymer processing. Initially, a sapphire window was used. Sapphire was found to have significant losses for the given temperature range using Wien's displacement law temperature modeling. In the wavelength this range stated earlier (4.83-9.66 μm) it was found that the

transmittance of sapphire drops from approximately 95% to practically zero, In this same range, the transmittance of zinc selenide holds steady at roughly 72%, as shown in Figure 2-3. Accordingly this sapphire window has since been replaced by a zinc selenide window.

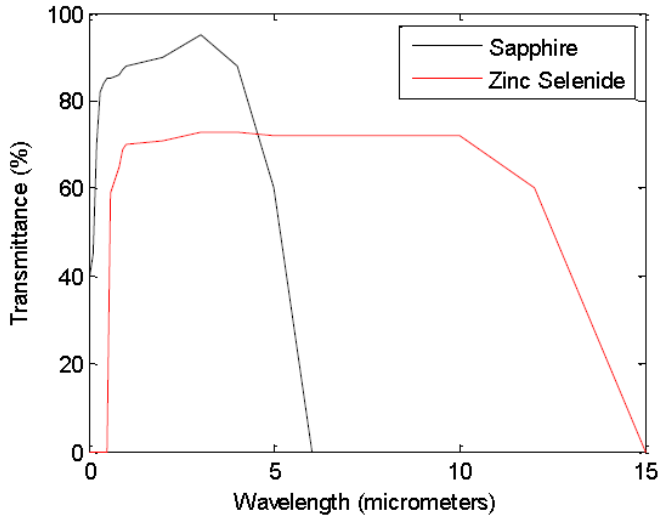

Figure 2-5: Transmittance of lens using sapphire and ZnSe

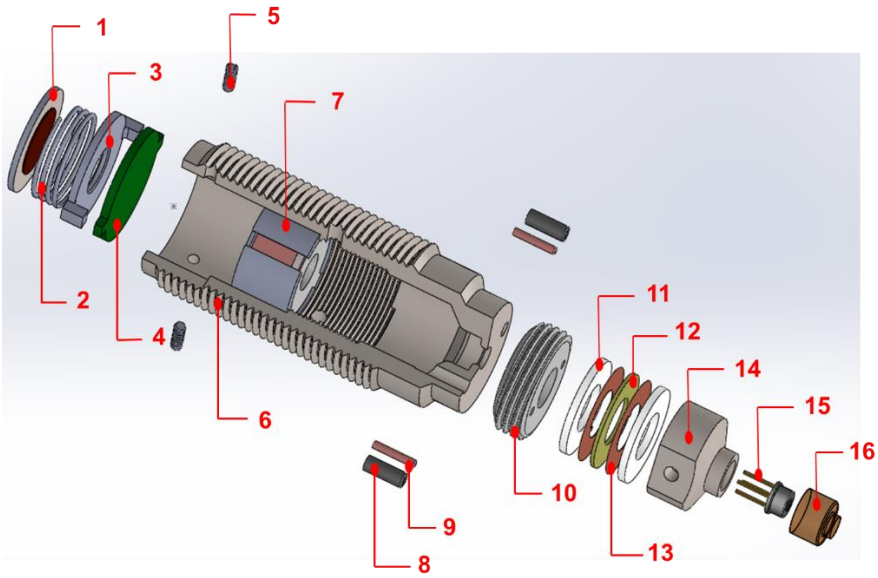

Figure 2-6: Mechanical packaging for multivariate sensing system

The sensor package is wrapped by a special designed metal case and smooth surface head enables a minimum marker print on the final product. Melt pressure during the polymer processing works on the piezoelectric ring through lens-stand off-PPS washer. A set screw is placed behind the second PPS washer

for supporting sensors. A special spring is designed according to an amount of force applied to the acoustic transmitter for well coupling between the transmitter and mold plate. For other details of the mechanical packaging, see Table 2-2 for list of components used in the sensor package.

Table 2-2: List of components for mechanical packaging

#	Component	#	Component
1	Transmitter	**9**	Charging probe
2	Spring	**10**	Set screw
3	End cover	**11**	PPS washer
4	Signal processing	**12**	PZT ring
5	End set screw	**13**	Copper layer
6	Sensor body	**14**	Front spacer
7	Battery package	**15**	HMS Z-11
8	Insulated tube	**16**	ZnSe lens

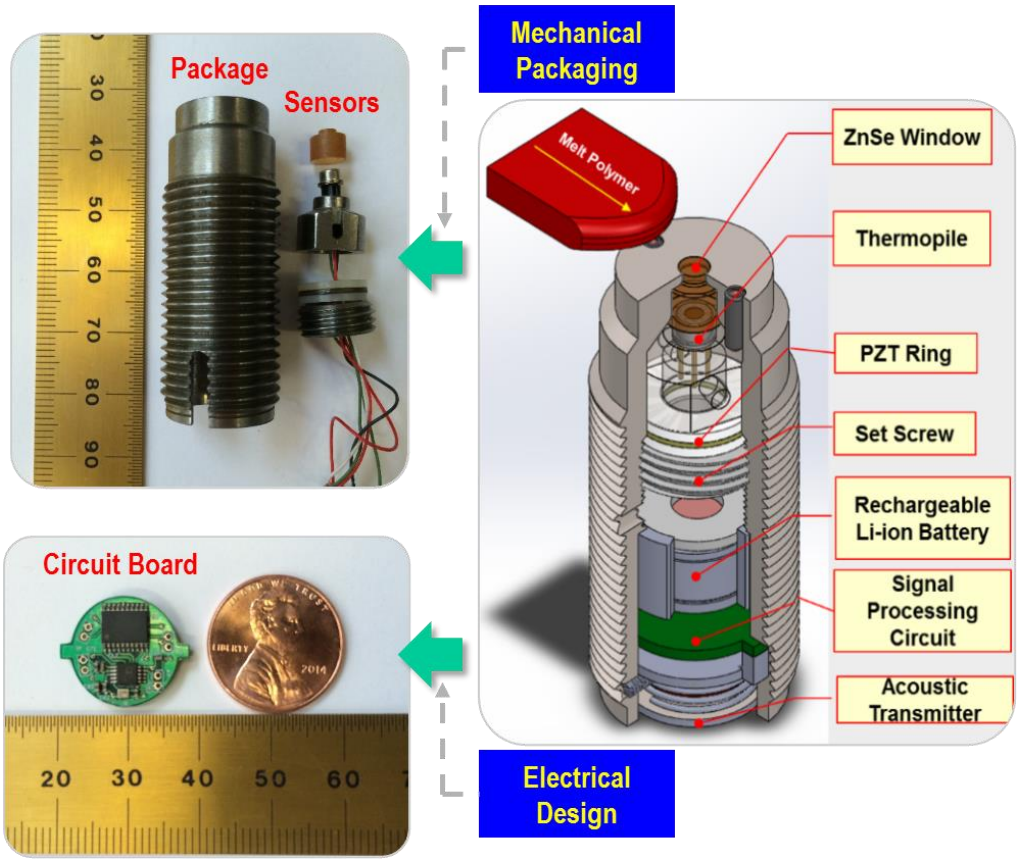

Figure 2-7: Multivariate sensor design and prototyping

Figure 2-7 shows the system proof-of-concept prototype, including both the printed circuit boards and the system final configuration. Specifically, the size of the MVS is 45 mm (height) × 20 mm (diameter). The MVS provides measurements of four key state parameters: 1) melt pressure; 2) melt temperature; 3) melt velocity; 4) melt viscosity and enabling acoustic wireless data transmission.

2.4 Summary

In this chapter, a multivariate sensor is designed, prototyped, and characterized with the capability of providing in situ feedback of four key in-process parameters: melt pressure, melt temperature, melt velocity and melt viscosity. Several fundamental aspects on instrumentation and measurement are presented concerning the design and performance evaluation of the wireless multivariate sensing system. Detailed analysis are performed for the design of the system hardware, including electronic design and mechanical packaging, to ensure the system functionality and robustness. The descripted new instrumentation's small size (45 mm × 20 mm), low power consumption (~20 mW), acoustic data transmission are suitable for long-term operation of polymer processing and RF-shielded environment, where electromagnetic wave cannot propagate through. Furthermore, the described MVS provides new capabilities for intelligent polymer processing, which is key to automated manufacturing system.

CHAPTER 3

MULTIVARIATE SENSING

3.1 Overview

Injection molding is a widely used mass-production manufacturing process to produce plastic parts. In each injection molding cycle, raw plastic materials are heated in a barrel, and forced into a mold cavity by a motor-driven screw under a high pressure (100 MPa or higher). The melt will then cool down in the mold cavity until it solidifies. Four key states of the plastic melt – pressure, temperature, velocity, and viscosity – are known to significantly affect the quality of the molded parts through the constitutive viscoelastic behavior of the polymer being processed. As a result, accurate measurement and control of these parameters are critical to preventing products from defects such as blistering (layered zones on the part surface due to high temperature of the melt), flow marks (wavy lines or patterns due to low melt velocity), or short shots [51,52].

Traditionally, the status of plastic melt inside the mold was estimated from the pressure and temperature measurement at external check points, e.g., on the screw motor, barrel, cooling water pump, nozzle, or mold clamp [53]. Numerical models then use the measured data as input to simulate the behavior of plastic melt flow inside the cavity [54]. Although the simulation model is capable of estimating the relative change of temperature or viscosity of the melt flow, it has shown to be difficult to accurately account for the temporal variations of the four parameters, due to the difference between the modeled and actual boundary conditions within a complex mold structure. The need for advanced sensing method to better monitor the molding process in real time has motivated researcher in recent years [55], and a dual-parameter sensor has been demonstrated that simultaneously measures both pressure and temperature of the plastic melt in the mold cavity, and send data to an external receiver through acoustic wireless communication [56]. For melt velocity measurement, the application of ultrasound wave has been investigated [56, 57]. An ultrasound sensor attached to the outside surface of the mold sends an acoustic pulse toward the polymer melt in the

mold cavity, through the mold steel. Due to the difference in material properties that affect the acoustic wave deflection, the amplitude of the acoustic pulse reflected by the interface between the mold steel and air (unfilled cavity) will be different from that reflected by the interface between mold steel and plastic. As a result, the location of the melt front can be calculated at the receiver's end by measuring the reflected acoustic wave amplitude. Another method investigated for velocity detection is the use of magnetic sensor, which detects the location of the melt front by measuring the magnetic field formed by a mobbing conductive flow [58]. While both methods are non-invasive, the accuracy of ultrasound detection decreases as the mold thickness increases, due to the diffusion of acoustic wave. Also, most of the plastic materials are non-conductive, thus cannot be detected using magnetic sensors.

Different methods have been investigated in order to measure the viscosity of a fluid. The capillary method defines viscosity based on the time for a specific amount of fluid to flow through a tube under a specific pressure, in the oscillating vessel method a specific force is applied to fluid in a vessel and fluid motion is damped due to the energy dissipation, then viscosity is measured based on the related time period for fluid motion decrement. Rotating cylinder method measures the fluid viscosity based on the induced torque to a cylinder where there is another coaxial rotating cylinder with a constant speed inside and fluid is filled between these cylinders [58-61]. In an injection molding process melt viscosity is in direct relation with pressure variation. Higher viscosity of the melt needs higher melt pressure for injection in the cavity and on the other hand lower viscosity results in flashing problem. Because of the difficulties in measuring direct viscosity of the melt, in traditional methods nozzle pressure was used as an estimated indicator for viscosity. This is due to the fact that the melt shear stress is in a direct relation with nozzle pressure and its shear rate is in direct relation with flow rate so viscosity is the ratio of nozzle pressure to injection rate and if the flow rate assumed to be constant the only variable is the nozzle pressure [62].

In this chapter, a new sensing method is proposed for the melt velocity and melt viscosity measuring in injection molding based on the measured temperature change and pressure change, shown in Figure 3-2. Melt velocity is calculated according to the melt temperature ramping rate, and time derivation of melt

pressure. The new MVS can detect melt pressure via a piezoelectric ring and melt temperature is measured via the installed IR detector in the sensor package.

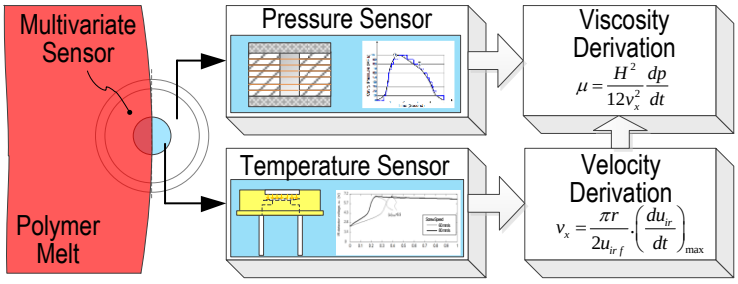

Figure 3-1: Illustration of sensor structure to calculation melt velocity and viscosity

3.2 Sensing principles

3.2.1 Pressure and temperature sensing

The melt pressure is sensed by acquisition of charge accumulated through the piezoelectric effect. The imposed stress on the PZT ring arises from compressive forces applied by the polymer melt to the zinc selenide lens. For a melt pressure, P, impinging on the lens with radius, R=1.5mm, the output voltage, V, is:

$$V = 4 \cdot g_{33} \cdot P \cdot H \cdot R^2/(OD^2 - ID^2) \quad (3\text{-}1)$$

where g_{33} is the voltage constant, H is the ring thickness of 0.5 mm, ID is the ring inner diameter of 4 mm, and OD is the ring outer diameter of 8 mm.

The MVS includes an HMSZ11-F5.5 thermopile from Heimann Sensor (Dresden, Germany) comprising a CMOS infrared detector having a diameter of 1.8 mm. The thermopile operates by measuring the incidence of radiation from the heated polymer melt. The thermal radiation, Q, is related to the fourth power of the temperature, T, the constant of proportionality, σ (the Stefan-Boltzmann constant equal to 5.67·10-8 $Wm^{-2}K^{-4}$), and the emissivity, ε, of the object according to the equation $Q=\varepsilon\sigma T^4$. The thermopile's output voltage, V, is also dependent on the reference temperature, TR, provided by an integrated thermistor:

$$V = k \cdot \varepsilon \cdot (T^n - T_R^n) \quad (3.2)$$

where k is the gain related to the infrared detector, and n is dependent on the filter and sensor characteristics

(*n* equals 4 for a perfect "black" characteristic and unlimited wavelength range). For the thermopile with a sensing area of 0.61 mm^2 and the zinc selenide lens of a transmittance of 0.8, an output voltage of 0.0186 V is anticipated for a melt temperature of 200 °C and a mold temperature of 20 °C, as calibrated [63].

3.2.2 Velocity and viscosity referencing

Figure 3-1 shows the senario when plastic melt is flowing across the sensor top from left to right. The *x* axis is represented by the straight line going across the center of the sensor along the melt flow direction. The point where the x axis intersects with the left boundary of the IR detector is defined as x=0. Based on the Stephan-Boltzmann law, the heat power rediating from an object is proportional to the fourth power of the object's temperature. This relationship is expressed as:

$$\phi_s = \varepsilon\sigma T^4 \tag{3-3}$$

where ϕ_s is the radiating power, ε is the emissivity factor of the melt, σ is the Stephan-Boltzmann constant and T is the melt temperature.

If all the radiation power is absorbed by the IR detector, the electrical charge generated by the sensing element, q, due to the pyro-electric effect, can be expressed as [9]:

$$q = \frac{p \cdot k \cdot \phi_s}{A_f\sqrt{G_T^2 + \omega^2 H_p^2}} A \tag{3-4}$$

Where t is the time, p is the pyro-electric coefficient, k is the loss factor of the IR radiation due to attenuation along the radiation path, A is the effective rediating surface area of the plastic melt (as shown in Figure 3-1), which is a function of tiem and $A_f$is the surface of the fully coverd lens, ω is the frequency of the infrared, and H, G_T, η are the thermal conductance, heat capacitance, and emissivity coefficient of the sensing element in the IR detector, respectively. Gernerally, a charge amplifier is used to convert the output charge of IR detector to a voltage output as:

$$u_{ir} = \frac{q}{C} = \frac{p \cdot k \cdot \phi_s}{C \cdot A_f \sqrt{G_T^2 + \omega^2 H_p^2}} A \tag{3-5}$$

where C is the feedback capacitance of the charge ampifier. It is seen from Eq. 3-5 that the parameters p, ω, H, G_T, η, are constants determinded by the pyro-electric material properties in the IR detector. Thus, the output voltage u_{ir} is dependent only on the effective radiating surface area A. Considering the fact that the width of the mold cavity (typicall wider than 20 mm) is much larger than the diameter of the IR detector (< 6 mm), the radiation surface area or the area of the lens exposed to the plastic melt, can be approximatedly expressed as a function of the melt front location x:

$$A = \frac{1}{2} r^2 2cos^{-1}\left(\frac{r-x}{r}\right) - (r-x)\sqrt{r^2 - (r-x)^2} \tag{3-6}$$

where r is the radius of the IR detector and the range of x is from 0 to 2r.

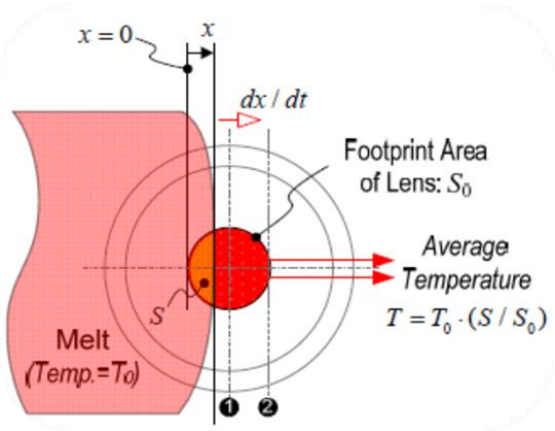

Figure 3-2: Schematic illustration of the polymer melt flowing over the lens

By taking the time derivative on both sides of the Eq. 2-4, the changing rate of output voltage du_{ir}/dt can be expressed as:

$$\frac{du_{ir}}{dt} = \frac{p \cdot k \cdot \phi_s}{C \cdot A_f \sqrt{G_T^2 + \omega^2 H_p^2}} \cdot \frac{dA}{dx} \cdot v_x \tag{3-7}$$

where $v_x = dx/dt$ is the velocity of the plastic melt front. From Eq. 3-6, it is seen that the derivative dA/dx has a maximum value when the condition $x=r$ is stratified. Assuming that the velocity v_x is

constant when the melt front flows through the IR detector, Eq. (3-6) can be written as:

$$(\frac{du_{ir}}{dt})_{max} = \frac{p \cdot k \cdot \phi_s}{C \cdot A_f \sqrt{G_T^2 + \omega^2 H_p^2}} \cdot 2r \cdot v_x \tag{3-8}$$

By substituting Eq. (3-5) into Eq. (3-7), the front velocity can be determined as:

$$v_x = \frac{\pi r}{2u_{irf}} \cdot (\frac{du_{ir}}{dt})_{max} \tag{3-9}$$

where u_{irf} is the voltage output from the charge amplifier when the IR detector is fully coved by the plastic melt, as described in Eq. (3-5) when $A=A_f$. In realistic injection molding processes, the value of u_{irf} and $(\frac{du_{ir}}{dt})_{max}$ can be measured from the output voltage signal and its time derivative. Thus, the melt front velocity can be determined according to Eq. (3-9).

The polymer's shear viscosity is a critical indicator of the polymer morphology, as well as a determinant of the residual stress distribution and resulting product quality. In order to calculate the melt viscosity and according to the rectangular shape of the cavity, melt flow is considered as a viscous flow between two fixed parallel plates. For a Newtonian incompressible flow between two parallel plates in a distance of H from each other as shown in Figure 3-3, Navier-Stokes equation is used for the x direction [64].

$$\rho(\frac{du}{dt} + u\frac{du}{dx} + v\frac{du}{dy} + w\frac{du}{dz}) = -\frac{dp}{dx} + \rho g_x + \mu(\frac{d^2u}{d^2x} + \frac{d^2u}{d^2y} + \frac{d^2u}{d^2z}) \tag{3-10}$$

The equation is solved in a two-dimensional space ($d/dz = 0$) and with the assumption of $v = w = 0$. So from the continuity equation we know the fluid velocity is just a function of z. Because of the incompressible fluid flow assumption, $du/dx = 0$, and the gravity force is also neglected in this problem, so the viscosity equation is shown as following equation:

$$\frac{dP}{dx} = \mu\frac{d^2u}{dz^2} \tag{3-11}$$

whereas the momentum equation in *z* and *y* directions follows the same mentioned assumptions, they lead to the pressure derivation equations with respect to *y* and *z* which both are equal to zero and as a result it can be inferred that the pressure is just function of *x*. Based on these results the two quantities on both sides

of Eq. (3-11) are independent and equal to a constant and can be solved by using the separation of variables method. Applying the boundary conditions for Eq. (3-11) and solving it the final equation will be:

$$\frac{dP}{dx} = \frac{12\mu v_x}{H^2} \tag{3-12}$$

where v_x is the average velocity of the fluid across the z axis. Eq. (3-12) can provide fluid viscosity in a Lagrangian frame of reference when the pressure is monitored at least in two points along the flow direction. In the new viscosity measuring method we use the basics of Eulerian specification of flow field, where the fluid motion is considered in a specific location as the fluid flows and time passes. So the time derivative of the monitored pressure from a single sensor is used as an input for the viscosity calculation. The relating equation is derived out by dividing the both sides of Eq. (3-12) by a factor of dt.

$$\mu = \frac{H^2}{12v_x^2}\frac{dP}{dt} \tag{3-13}$$

where dP/dt is the time derivation of the melt pressure as the melt passes the centerline of the sensor. Although pressure sensor does not provide data about the time by when melt front passes the centerline of the sensor, but the mentioned time can be considered from the velocity sensor due to the fact that these two sensors are coaxial in the multivariate sensor structure.

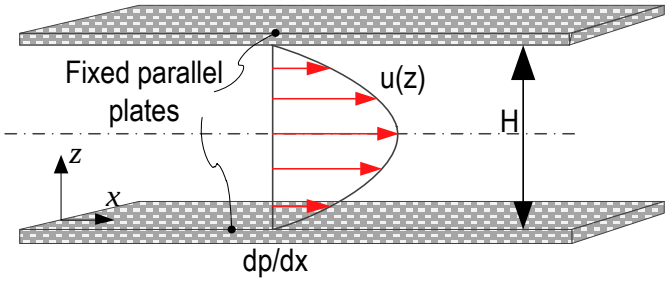

Figure 3-3: Velocity profile of incompressible viscous flow between two fixed parallel plates

3.3 Experimental Evaluation

3.3.1 Design of experiments

An ASTM test mold with an instrumented flex bar cavity was used for this study, as shown in Figure 3-4. The cavity contains a piezoelectric pressure transducer (Priamus 6001A, Schaffhausen, Switzerland) near the gate. At the end of the cavity there is an exposed type-N thermocouple (Primaus 4001A) as well

as an infrared melt pyrometer (Omega OS1562, Stamford, CT). The MVS was installed at the center of the cavity. This mold was installed on a fully electric injection molding machine (Sumitomo SE75DUZ). Four machine signals (injection pressure, screw position, screw speed, and screw RPM) as well as data from the commercial sensors were acquired via a Priamus eDAQ 8102A at 500 Hz. Data from the MVS was acquired through acoustic data transmission at a rate of 500 Hz.

A 12-run blocked half-fractional DOE, a design of $3\times2^{3-1}$ as shown in Table 3-1, was implemented to investigate the effects of melt temperature, mold temperature, packing pressure, and injection velocity. The polymer resin was high impact polystyrene (HIPS, Dow Styron 478). During experimentation, time was allowed for the machine to reach the set points for the melt and mold temperature. The injection molding machine was then operated for fifteen minutes before collecting samples to ensure the process reached steady-state. Twenty samples were then collected for each run.

Table 0-1: Blocked Half-Fractional Design of Experiments (DOE)

Run	T_{melt} (°C)	T_{mold} (°C)	P_{pack} (MPa)	v (mm/s)
1	190	21	30	10
2	190	21	30	40
3	190	21	30	100
4	190	60	50	10
5	190	60	50	40
6	190	60	50	100
7	220	60	30	10
8	220	60	30	40
9	220	60	30	100
10	220	21	50	10
11	220	21	50	40
12	220	21	50	100

3.3.2 Data analysis

Figure 3-4 illustrates an overview of sensor location installed in flex bar mold cavity, where typical molding traces for the injection molded product are shown in the graphs obtained through the measurements of different types of sensor. Typically, there are eight traces corresponding to different location's measurement for either temperature or pressure. Graph 1-3 are measurements for mold temperature, melt

pressure, and melt temperature from MVS located in middle of the cavity; graph 4 is measurement for in-mold temperature from Priamus cavity thermocouple installed at the end of cavity; graph 5 is obtained by Omega IR near the end of cavity for measuring melt temperature; graph 6 is nozzle pressure measured by Priamus nozzle sensor; graph 7 is the runner pressure and graph 8 is the Priamus gate pressure.

As the melt polymer flowing through the cavity: first reaches the runner sensor, then the gate pressure sensor, and finally the MVS, there is a significant pressure drop at the peak value between each sensor due to the viscosity of the melt and its flow resistance. Also a significant pressure decay remains in the packing stage. At around 10 s, the packing stage ends. The drop in the runner pressure at this instant indicates that the melt in the feed system is still semi-molten. No similar drop is seen in the cavity, indicating that the gate is fully solidified. Comparing the melt temperature measured by the MVS to that of the IR detector, shown in graph 1 and 5 of Figure 3-4, it is seen that the MVS detected the arrival of the melt before IR detector, and with a slightly higher reading. This is because the commercial pyrometer measures the intensity at a single wavelength and thus has a minimum temperature of 80 ℃, clapping the process data at the start and end of its readings. By comparison, the MVS admits a wide wavelength range and captures a more complex temperature behavior, such as the cooling of the melt in the mould cavity. The mold temperature from MVS is for melt temperature measurement compensation, which also shows a 10 ℃ temperature change indicating an expected behavior for it is isolated from the melt by the 5 mm height of the window lens. The otherwise good agreement between MVS and the commercial sensor validates the functionality of the MVS.

The true velocity of the melt cross over the MVS is unknown, it can be well estimated in the follow ways. One method to estimate the melt velocity can be used as the product of the ram velocity, V_{ram}, with the ratio of the ram to cavity cross-section area. The molding machine's ram has a diameter of 28 mm while the cross-section dimensions of the cavity are 12.25 mm wide by 3.13 mm thick. Neglecting compressibility, one should expect about 16 mm/s of melt velocity in the cavity per 1 mm/s of ram velocity. Another approach is to estimate the melt velocity from process data acquired by multiple in-mold sensors. There is

a known distance, Δx, between the sensors as well as a known travel time, Δt, for the polymer melt to reach the downstream sensor, so the melt velocity can be calculated as:

$$v_{melt} = \frac{\Delta x}{\Delta t} \tag{3-14}$$

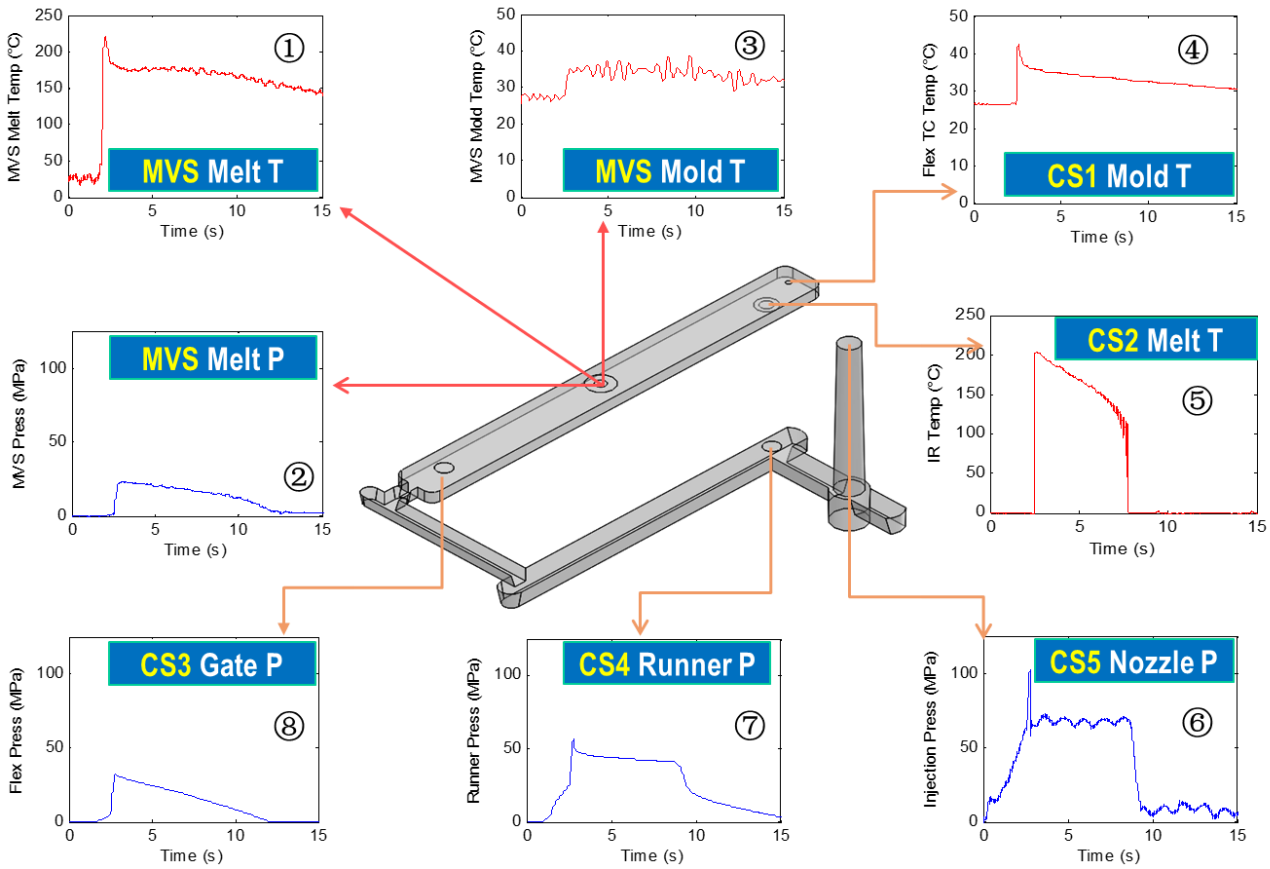

Figure 3-4: Overview for sensor location in flex bar mold cavity (CS: commercial sensor)

Given the potential for velocity estimation errors from polymer compressibility, the melt velocity was calculated from the time for the melt to travel from the piezoelectric cavity pressure sensor to the multivariate sensor, noted as PC→PMVS.

The true velocity of the polymer melt in the mold cavity can be well estimated by dividing the distance between the Priamus and MVS pressure sensors by the difference in the melt arrival time, i.e. *dx/dt*. The correlation between the melt velocity and the slope of the melt temperature is shown in Figure 3-5; Figure 3-5 suggests significant correlations with a coefficient of determination, R2, of 0.905 for slow injection velocity runs. Error exist when fast injection velocity occurs.

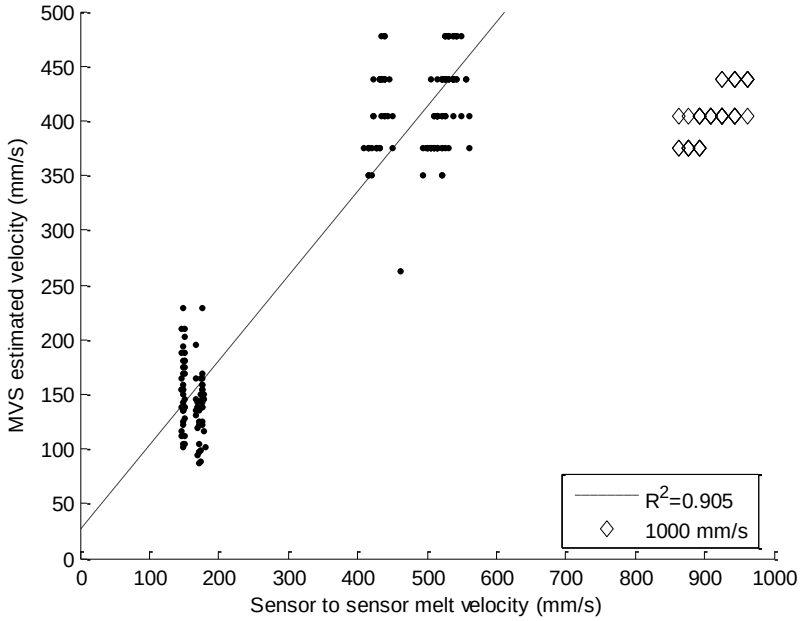

Figure 3-5: comparison of velocity estimation between MVS and sensor to sensor model

Capillary rheometry was performed for this neat high impact polystyrene (Dow Styron 478 ®) having a melt flow index (MFI) characterized according to ASTM D-1238 of 6.0 g/10min and a density of 1.036 g/cm3. For this investigation, a Dynisco (Franklin, MA) LCR7000 capillary rheometer was used to measure viscosity in compliance with ASTM D3835-08 for shear rates ranging from approximately 1 to 16,000 inverse seconds at three different temperatures of 190° C and 220° C. The capillary length and diameter were respectively 30 and 1 mm. The Cross-WLF model described by equations listed in [31] was fit with the resulting coefficients and statistics provided in Table 3-2.

Table 3-2: Cross-WLF model coefficients for PS

Coefficient	*Value*
n	0.281
τ^* [Pa]	$23.6 \cdot 10^3$
D_1[Pa·s]	$9.00 \cdot 10^{12}$
A_1 [K]	31.1
A_2 [K]	51.6
Correlation	0.9854
R^2	0.9733

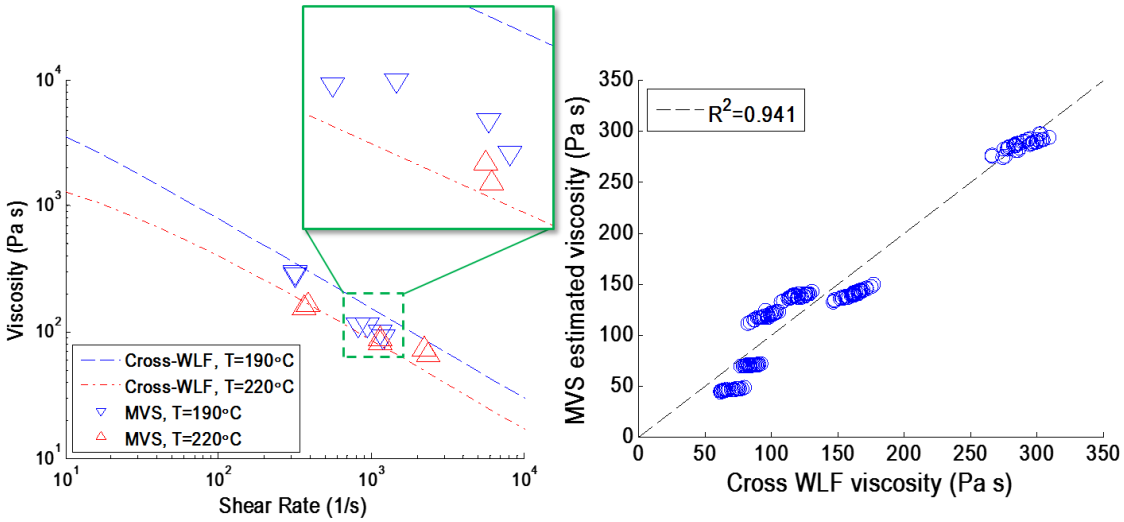

(a) (b)

Figure 3-6: Rheological model and in-mold apparent viscosity of PS

The viscosity estimation by the MVS is based on the transient pressure signal and the estimated velocity. The resulting viscosity estimations are compared to the characterized viscosity in Figure 3-6; both the viscosity and shear rate values are derived solely from the MVS without any other sensor or machine data. The results show that the MVS's viscosity estimation are of a correct order of magnitude and exhibit some of the expected behavior regarding shear thinning dependence. The temperature dependence of the apparent viscosity as estimated by the MVS is not consistent with that predicted by the Cross-WLF model. This is because the temperature of the flowing polymer melt in the mold cavity is only loosely correlated with the molding machine's set barrel temperature. Lower barrel temperatures may provide an initially cooler melt having a greater viscosity that will tend to increase the polymer melt temperature through shear heating. As such, the polymer melt temperature is as strongly dependent on the injection velocity as the barrel temperature. Another reason is that the apparent viscosity will also depend on the development of the solidified layer. The thickness of the solidified layer will be dependent on the injection velocity, melt temperature, and mold temperature so as to induce variances in the apparent viscosity. However, the MVS'

estimates of in-mold melt viscosity remain useful with respect to verifying process, material, and product consistency.

3.4 Summary

The proposed multivariate sensor (MVS) in this chapter could provide online in-process measurements of melt temperature and melt pressure with accuracies comparable to commercial sensors. Estimated melt velocity from MVS data shows a good coefficient of determination, R^2, equal to 0.939, across all cycles with results from the sensor-to-sensor model. The remaining estimation error is caused by the slow response during the melt temperature sensing, thus failing to track fast melt polymer flowing across the lens. The viscosity estimation from the MVS data based on melt temperature and pressure change during the polymer processing. The polystyrene material used in this experiment was characterized using a capillary remoter. The results indicate that the apparent viscosities estimated by the MVS are on a good correlation with those characterized and fit to the Cross-WLF model. Shear thinning behavior could be observed, though melt temperature dependence of the viscosity is inconsistent.

CHAPTER 4

ACOUSTIC-BASED MULTI-PARAMETER TRANSMISSION

4.1 Overview

Ultrasonic wave have been widely explored as varying means to acquire data. No-Destructive Testing (NDT) techniques are one example of using ultrasonic waves to detect damage or monitor health in machine tool, workpiece, or structures. The basis for NDT is the principle of pulse-echo reflection. Acoustic wave generated by a piezoelectric transducer is coupled to the test specimen and propagated through the material. Part of the acoustic wave energy is reflected when the wave encounters a fracture or an inhomogeneous region in the material. This reflection characterizes the discontinuity in the monitored structure [66].

Acoustic waves have also been investigated for image acquisition in medical applications [67], and geometrical measurement in metrology [68]. Wave formats vary but include (1) A-scan, where the presentation is based on the amount of received ultrasonic energy as a function of time, (2) B-scan, which is based on the A-scam method as the probe moves, and provides a cross-section view of the test specimen, or (3) C-scan, where both signal amplitude and the time-of –flight (TOF) are recorded to provide a plan view of the specimen features. Acoustic waves have further been explored for real-time manufacturing process monitoring, e.g., in detecting cracks in machine structures [69] or characterizing surface properties [70].

The pulse echo method is limited in conveying details of locally measured process states. Fig. 1 illustrates examples of manufacturing processes that may benefit from an acoustic wave-based data transmission method. For this purpose, acoustic sensor are placed at critical locations on the machine for transmitting state information during the respective manufacturing process, in real-time, to provide input for enhanced process control. Previous research [71] has demonstrated the feasibility of such a wireless data transmission method in RF-shielded environments, where the electromagnetic waves are not able to propagate. This technique opens up the possibility of integrating acoustic sensors into machine tools in various manufacturing processes, without the need to drill holes through the machine structure to

accommodate sensors cables, thus minimizing effect on the structural integrity of the machines being monitored.

In examples shown in Fig. 1, parameters measured by sensors may be encoded in a purposefully modulated acoustic signal for transmission through representative machine structures in the categories shaping (e.g., drilling), forming (e.g., stamping), or primary shaping (e.g., injection molding) [72]. Such acoustic signal transmission, however, is subject to potential data loss due to wave reflection and attenuation. This chapter investigates the effect of several parameters on the accuracy and reliability of acoustic wave-based signal transmission, such as carrier frequency, bandwidth, signal-to-noise ratio, data bit rate, and transmitter-receiver misalignment. In Section 4.2, the analytical background of acoustic wave propagation and radiation is briefly introduced. Section 4.3 presents the model and numerical solution for wave propagation on the ANSYS platform. Section 4.4 describes the experimental evaluation of the simulation results, for a range of conditions. In the last section, conclusions are drawn.

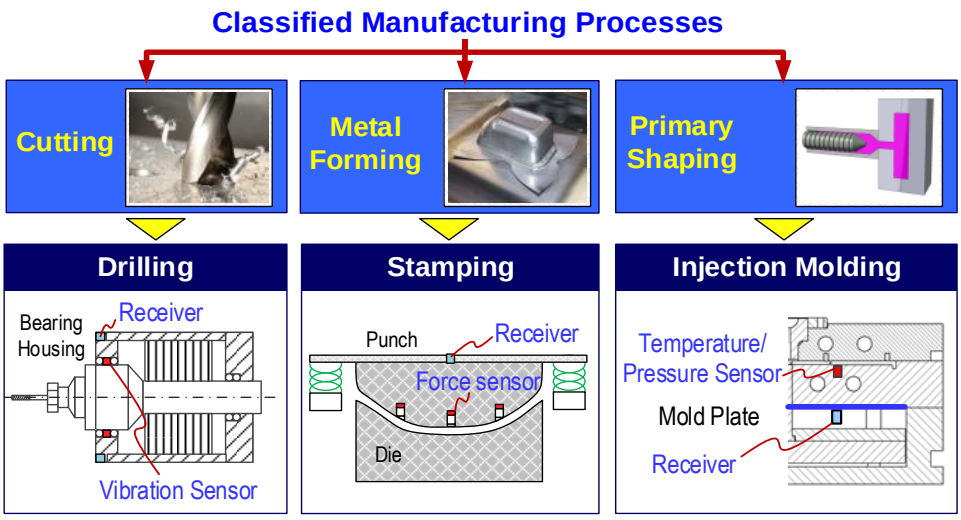

Figure 4-1: Manufacturing processes as potential candidates for acoustic-based wireless data transmission

4.2 Acoustic Modulation and Wave Propagation

4.2.1 Coded-wave modulation

To transmit measured parameters to a data receiver outside of a metallic structure, acoustic waves have been investigated as an information carrier [70]. Fig. 2 illustrates the process of signal modulation transmission, and demodulation, where each of the measured parameters is converted into a digital packet, consisting of "1's" and "0's". Multiple carrier frequencies (f_1 to f_3) are strategically modulated to encode digitized data [71]. The transmitted signal is subsequently demodulated on the receiver's end through a wavelet transform for parameter extraction.

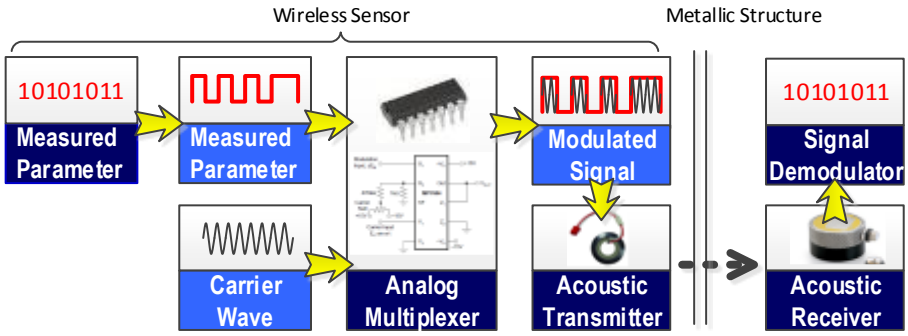

Figure 4-2: Acoustic modulation for wireless data transmission

4.2.2 Wave equation and characteristics

Acoustic transmission occurs in 3D space with the potential for multiple acoustic point sources. A circular plate is selected to serve as the acoustic transmitter and the pressure in any point of the propagating environment can be described by modelling the transmitter as an infinite number of small elements wherein each of them performs as a simple point source that vibrates with the speed of $U_0 e^{jwt}$. The geometry and coordinates of the transmitter are shown in Figure 4-3. The total pressure generate by these point sources can be expressed as [73]:

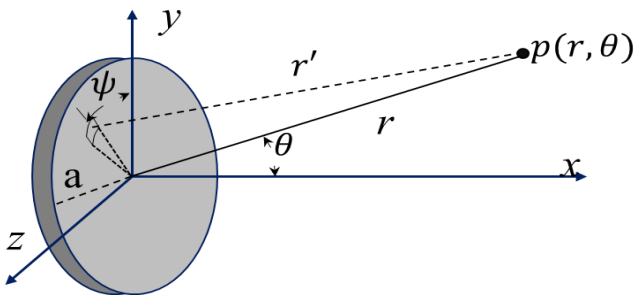

Figure 4-3: Geometry used to represent the circular ultrasonic transmitter

$$p(r,\theta,t) = j\rho_0 c \frac{U_0}{2\pi} k \int_s \frac{e^{j(\omega t - kr)}}{r} ds \tag{4-1}$$

where r is the distance from the transmitter surface to any point in the space, ρ is the density, U_0 is the amplitude of vibration at the disk surface, c is the sound speed in the medium, ω is the radian frequency and k is the wave number which is equal to ω/c, and s is the surface of the transmitter disk. The acoustic wave along the normal from the disk center where $\theta = 0°$ can be calculated with the complex ultrasonic pressure as:

$$p(r,0,t) = 2\rho c U_0 e^{jwt}[\mathrm{e}^{-\mathrm{jkr}} - \mathrm{e}^{(-\mathrm{jk}\sqrt{r^2+a^2})}] \tag{4-2}$$

And the amplitude of the pressure is the magnitude of the above expression, obtained as below:

$$p(r,0) = 2\rho c U_0 \left| \sin\left\{ \frac{1}{2} kr[\sqrt{1+(\frac{a}{r})^2} - 1] \right\} \right| \tag{4-3}$$

It can be seen that, due to the nature of the sine function, the pressure along the axis of the transmitter fluctuates between 0 and $2\rho c U_0$. Thus we called the region within which the pressure fluctuates near field. As the distance r increases, the maxima and minima of the pressure become more widely spaced. However, if r is large enough such that $r/a \gg 1$ and $r/a \gg ka$, the pressure along the x axis can be expressed as [8]:

$$p(r,0) = 2\rho c U_0 \frac{a}{r} ka \tag{4-4}$$

This means the acoustic pressure exhibits a monotonically decreasing behavior with a $1/r$ dependence. This region is called the far field. For the fluctuating pressure distribution in the near field, seen in Figure 4-4, it is very likely for the receiver placed within the near field to receive week signals. Therefore, for the injection mold cavity with fixed mold thickness, the combination of the frequency a radius of the transmitter needs to be chosen carefully to avoid generating a near field that is longer than the thickness of the typical injection mold. It can be seen that the last maximum pressure marks approximately the end of the near field. The near field changes into the far field at a distance N from the transmitter surface, this distance can be approximated as:

$$N = \frac{a^2}{\lambda} - \frac{\lambda}{4} \tag{4-5}$$

where λ is the wavelength of the generated acoustic wave. The range of the near field as a function of frequency is plotted in Figure 4-5 for $a = 2$, 5, 8, and 10 mm. It is clearly shown in Figure 4-5 that the range of near field increases with increasing of both frequency and radius. For the injection molds with fixed thickness, to avoid the placement of the receiver within the near field and thus reception of weak signals, the radius of the transmitter needs to be selected carefully. For example, if the frequency range of 0.5 – 2.0 MHz that is used throughout the data transmission, a transmitter radius of up to 11 mm is chosen for the mold thickness of up to 45 mm.

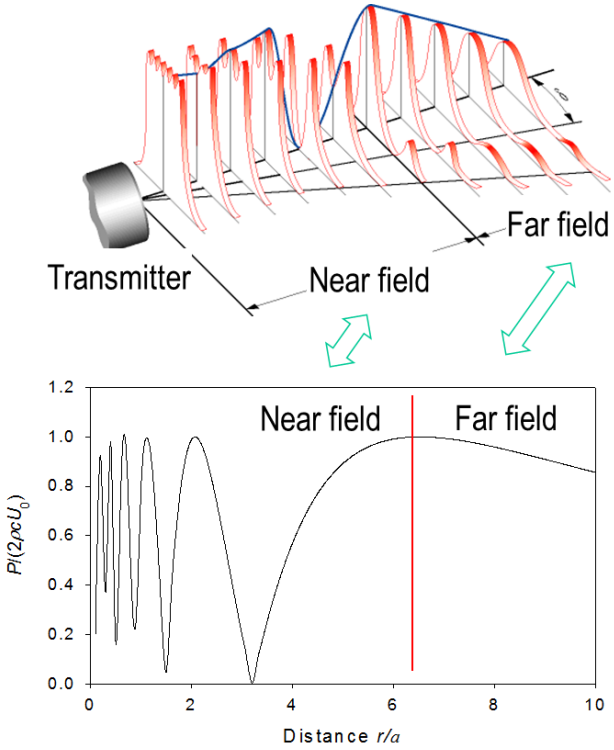

Figure 4-4: Illustration of the axis response in near field and far field

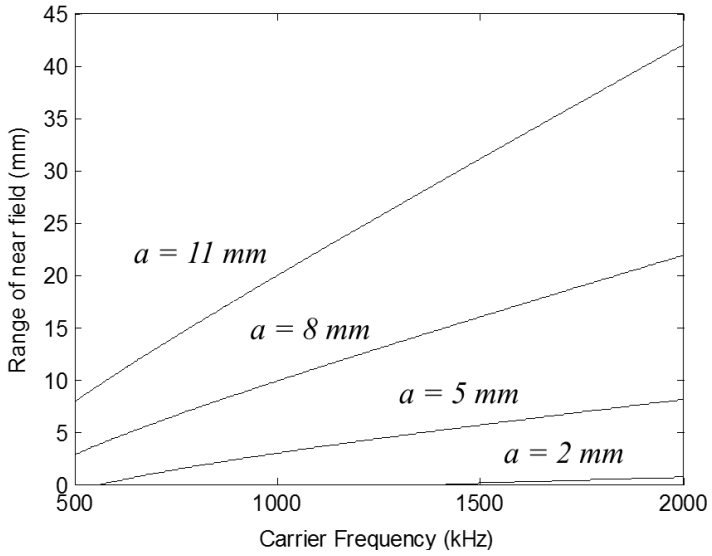

Figure 4-5: Range for near field at different carrier frequencies

In the far field, the pressure varies not only along the different directions but also across the axial axis, thus exhibiting a strong angular dependence, called the beam pattern. The total acoustic pressure at any point in the space can be obtained by integrating the acoustic pressure generated by the line sources [8]:

$$p(r,\theta,t) = j\frac{\rho c}{2}U_0\frac{a}{r}kae^{j(\omega t-kr)}\left[\frac{2J_1(ka\sin\theta)}{ka\sin\theta}\right] \tag{4-6}$$

where $J_1(*)$ is the Bessel function of order 1. The amplitude of the acoustic pressure can be expressed as:

$$\mathrm{P}(r,\theta) = \sqrt{2}\left|\frac{\rho c}{2}U_0\frac{a}{r}ka\left[\frac{2J_1(ka\sin\theta)}{ka\sin\theta}\right]\right| \tag{4-7}$$

To illustrate the angular dependence, examples of the beam pattern for four different ka combinations are plotted in Figure 4-6, where the acoustic pressure is converted to the decibel as shown below:

$$P_{dB}(r,\theta) = 20\log\frac{P(r,\theta)}{P(r,0)} \tag{4-8}$$

In the Figure 4-6, we fix the radius of transmitter $a = 10$ mm, and vary the frequency of carrier wave with $f_1 = 500$ kHz, $f_2 = 1000$ kHz, $f_3 = 1500$ kHz, and $f_4 = 2000$ kHz.

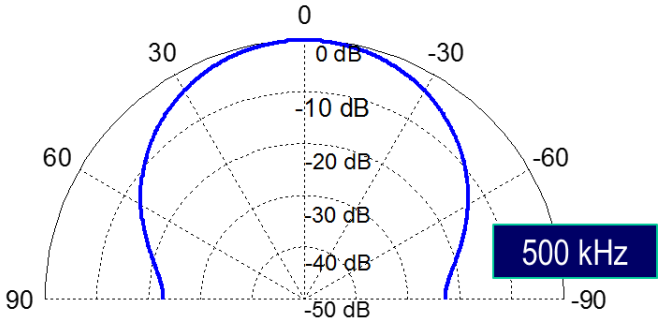

(a) $f_1 = 500$ kHz

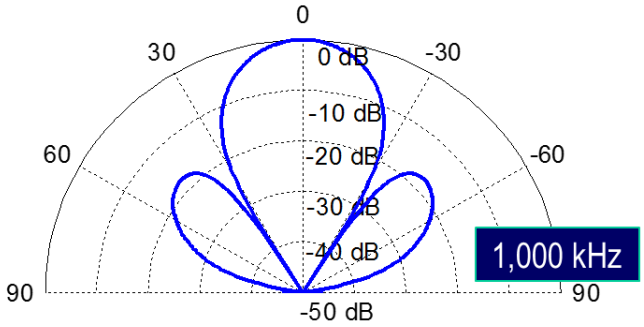

(b) $f_2 = 1000$ kHz

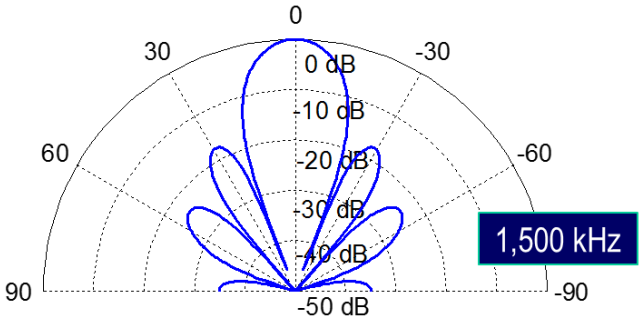

(c) $f_3 = 1500$ kHz

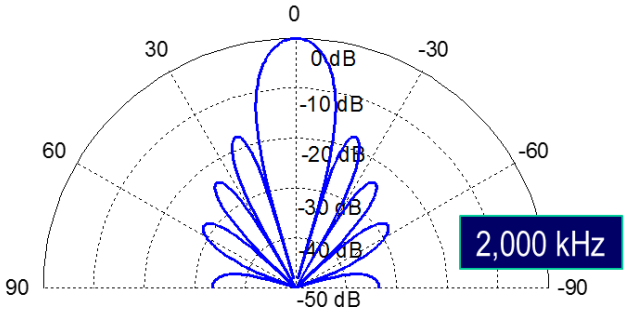

(d) $f_4 = 2000$ kHz

Figure 4-6: Beam patterns for the circular transmitter

Figure 4-6 shows the relative strength and angular dependence of the acoustic pressures. Take the Figure 4-6 (b) as an example, the pressure maximum is located on the transmitter axis, namely $\theta = 0°$. As the angle increases, the acoustic pressure decreases until drops to zero at an angle $\theta_1 = 30°$. The conical shape within θ_1 is called the main lobe of the beam pattern. Further increasing the angle will result in a pressure increase to its second peak, after which the pressure drops to zero again, which generates a second largest peak. The main lobe is of considerably larger strength than the side lobes, therefore the angle θ_1 is usually used as a measure of the solid angle of the space that is strongly affected by the sound pressure of the transmitter.

4.2.3 Wave propagation in typical structures

In general, the typical structures constituting machining tools can be the representatives shown in the Figure 4-7, including rectangular structures and angled structures. Those structures are very popular in all different kinds of machines for their easy manufacturing and high stability. Typically, each of these two typical structures constitutes of two case studies. For rectangular structure, we study the face-to-face case and perpendicular case, illustrated in details in the left part of Figure 4-7, while for the angled structure, we study the face-to-face case and end-to-end case, shown in details in the right part of Figure 4-7. In these different case studies, we fix the position of transmitter and move the receiver at different locations to investigate received signal strength, which is of critical important to the received signal outside mold cavity with high signal-to-noise-ratio (SNR), thus enabling successfully acoustic-based data transmission.

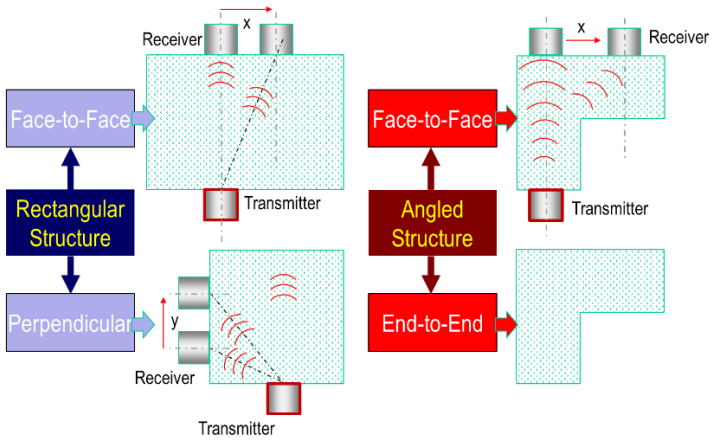

Figure 4-7: Typical structures in machine tools

1) Face-to-face arrangement

In this case study, the transmitter is placed in the middle of one side of rectangular structure while the receiver is moving from the opposite location on the face-to-face side to further right or left locations. It's clear in the Figure 4-8 that the signal amplitude decreases as the receiver misaligns with the transmitter axis to the further right or the left within a certain distance. It drops to zero at certain distance and arrive to the second largest peak as the receiver move further right or left. We can also see that the received signal amplitude increases when receiver is aligned with transmitter. Figure 4-8 illustrates received signal strength under different carrier frequencies,

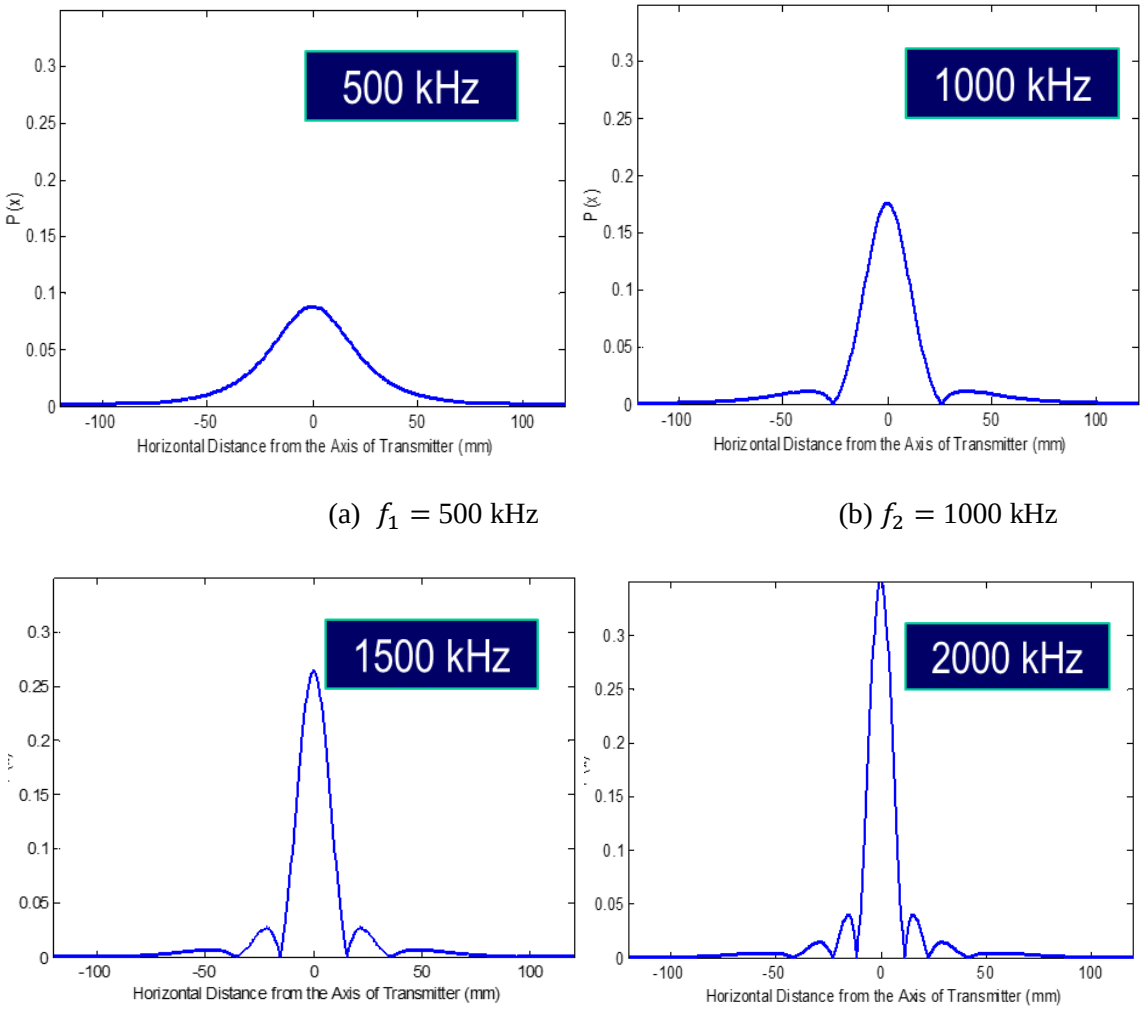

(a) $f_1 = 500$ kHz (b) $f_2 = 1000$ kHz

(c) $f_3 = 1500$ kHz (d) $f_4 = 2000$ kHz

Figure 4-8: Received signal strength estimation in face-to-face arrangement

namely $f_1 = 500$ kHz, $f_2 = 1000$ kHz, $f_3 = 1500$ kHz, and $f_4 = 2000$ kHz, at different receiver locations. The fluctuated received signal strength along the face-to-face side is interacted through the effect of main or side lobes illustrated in Figure 4-6. During the wireless acoustic data transmission, the receiver should be placed as closely as to the transmitter axis, to avoid these zero pressure location for the placement of receiver, thus ensuring a high SNR signal on the outside of metallic shield.

2) Perpendicular Arrangement

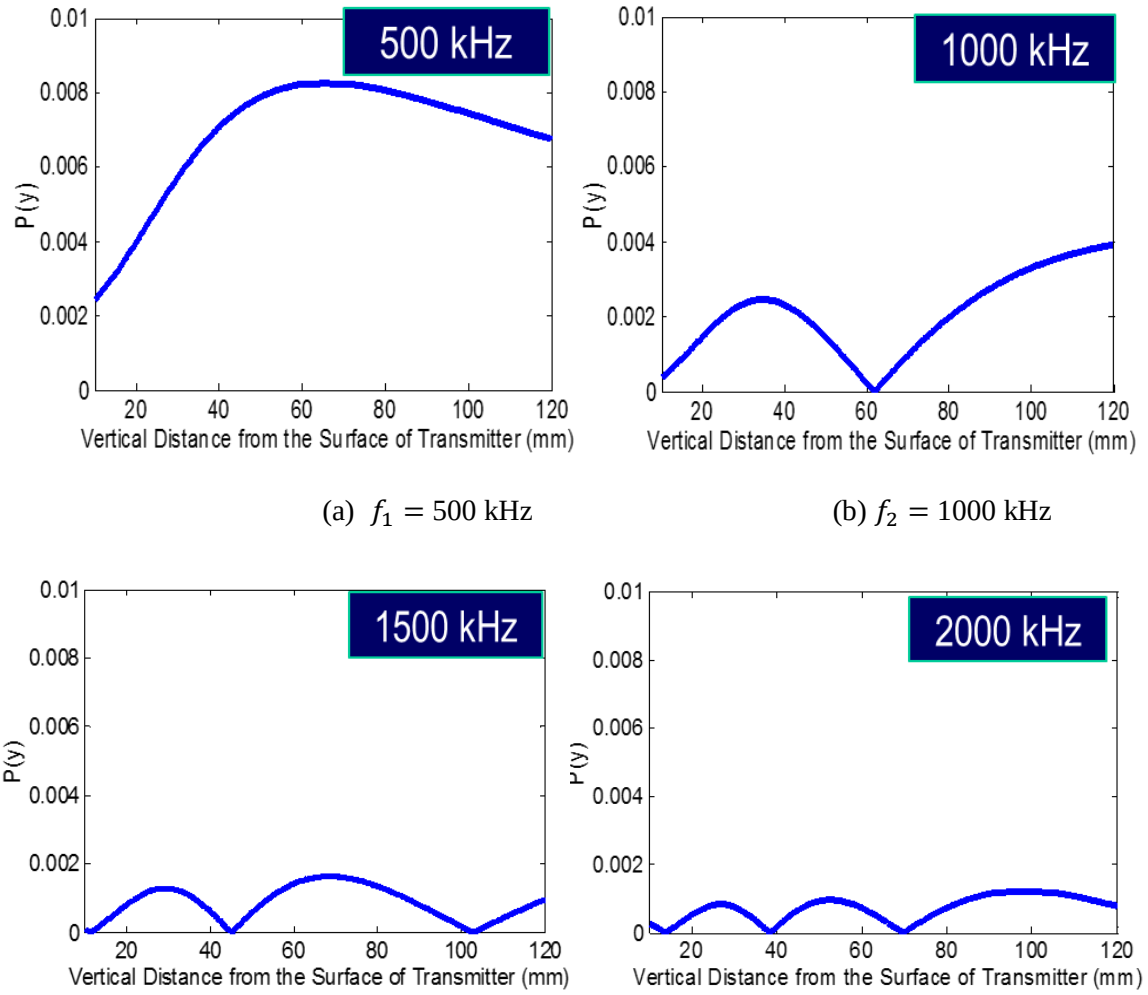

(a) $f_1 = 500$ kHz (b) $f_2 = 1000$ kHz

(c) $f_3 = 1500$ kHz (d) $f_4 = 2000$ kHz

Figure 4-9: Received signal strength estimation in perpendicular arrangement

In this case study, the receiver is placed along the perpendicular side of the rectangular structure while the transmitter is fixed at the horizontal center location. It's clear that amplitude of the received signal depends on both wave intensity and incident angle (angle between the transmitter axis and receiver axis) as different receiver locations. The location of maximum amplitude of signal can be analytically determined under different carrier frequencies. From the Figure 4-9, the zero pressure location is caused by the separated main or side lobes.

3) Effect of diffraction

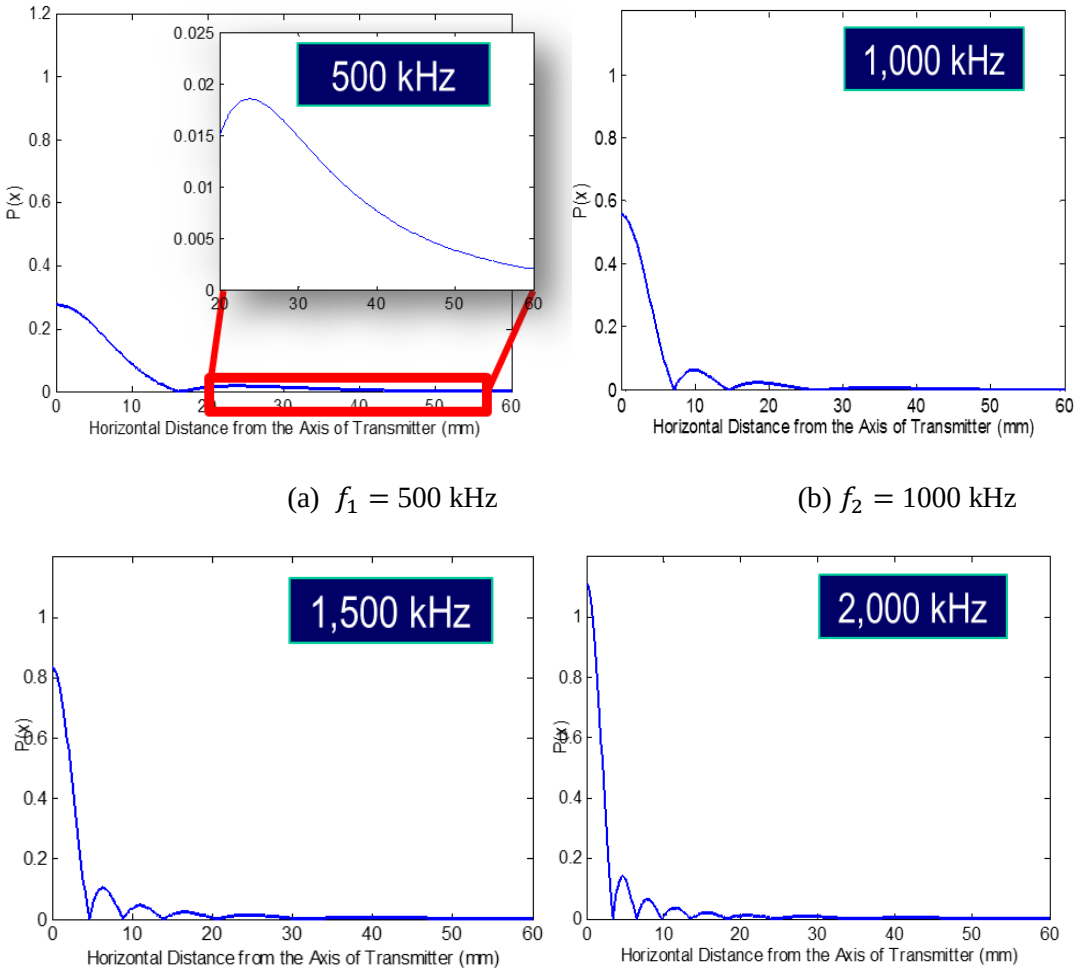

(a) $f_1 = 500$ kHz (b) $f_2 = 1000$ kHz

(c) $f_3 = 1500$ kHz (d) $f_4 = 2000$ kHz

Figure 4-9: Effect of diffraction on received signal strength

In this case study, the transmitter is placed at one end of the angled structure and the receiver is moving the side at different locations. The spatial distribution of signal strength varies as the carrier

frequency increases. It is feasible to achieve signal transmission in angled structure through leveraging diffraction according the characteristics of each structure.

4.4 Experimental Evaluation

To evaluate the analytical results under different cases in the Section 4.3, acoustic-based wireless data transmission has been tested on a representative production level machine (Sumitomo SE75DUZ injection molding machine), as shown in Figure 4-10. Acoustic wave is generated and received using a pair of C1007 Olympus transducers. The receiver is installed on the back surface of a 40 mm thick steel plate, by using a set of sensor holders to maintain consistent coupling between the plate and receiver. To investigate the effect of alignment between the acoustic transmitter and receiver on data transmission, the sensor holder is designed to allow the transmitter and receiver to be misaligned from each other within a range of 0-40 mm. Based on the frequency of acoustic wave in the steel material [5], the carrier frequency is chosen in the range of 1.2-1.8 MHz for a signal channel data transmission with 8 digits. To evaluate the quality of signal received by the transducer on the back of the mold, the power of the signal strength is calculated by averaging the power of frequency components that is equal to the carrier frequency, which is expressed as

$$p_{\text{signal}} = avg(p_f) \tag{4-9}$$

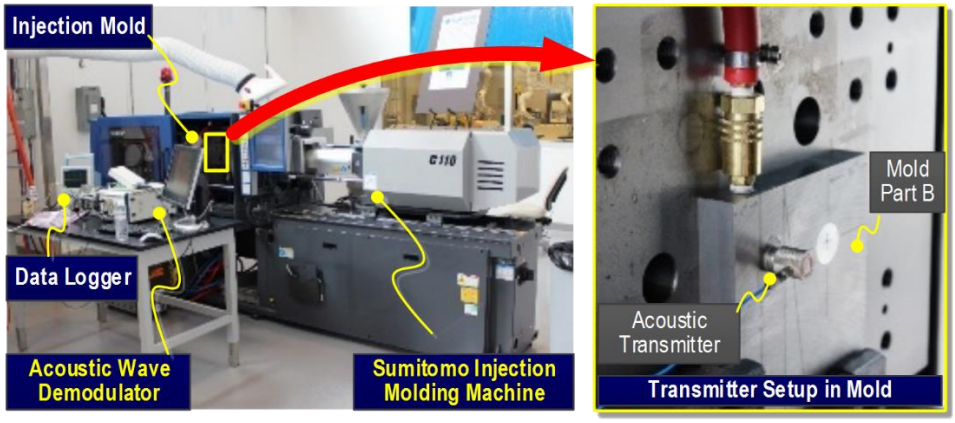

Figure 4-10: Acoustic-based data transmission experimental test set-up

Carrier frequencies (f_i, $i = 1, 2, 3, 4$) of 1.2, 1.4, 1.6, and 1.8 MHz are investigated in both the analytical and experimental study. The axial misalignment between the transmitter and receiver is varied

by 0-40 mm, with 5 mm increments. For each setting, the experiment is repeated 20 times to characterize the measurement repeatability. The calculated and measured signals as a function of the misalignment (represented by the lateral, *x*-position) are plotted in Figure 4-11, where the red line corresponds to the calculated signal strength, and the measured signals at different locations are illustrated in blue bar.

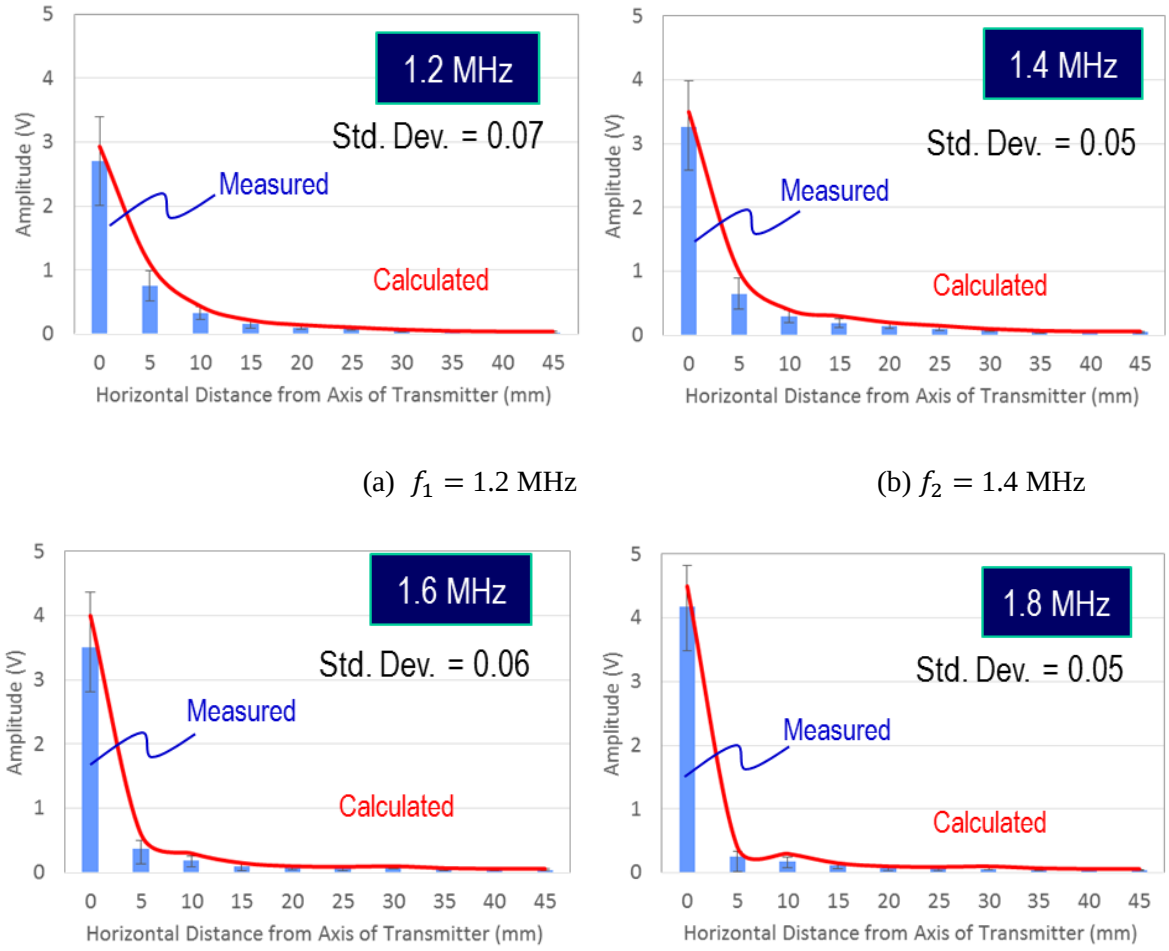

(a) $f_1 = 1.2$ MHz (b) $f_2 = 1.4$ MHz

(c) $f_3 = 1.6$ MHz (d) $f_4 = 1.8$ MHz

Figure 4-11: Calculated and measured signal strength (Unit of lateral position, *x: mm*)

Figure 4-11 shows that the received signal strength scattered along *x* direction when carrier wave is in low frequency, indicating that it is feasible for non-aligned data transmission. While for high frequency carrier wave, the received signal strength concentrated along the axial direction of the transmitter, suitable for aligned transmission.

Figure 4-12 shows the experimental set up for face-to-face transmission in angled structure, where the length of arm is 45 mm, constructing a 90 ° angle. During the experiments, 500 kHz, 600 kHz, 800 kHz, 900 kHz are used as the carrier wave frequencies for acoustic-based data transmission. For each case, the misalignment between the transmitter and receiver was varied by 0 – 45 mm, with 5 mm increments. For each setting, the experiment was repeated 20 times to characterize the measurement repeatability. The red line corresponds to the calculated value from the analytical model, while the mean value during each setting was highlighted in blue bar. Standard deviation is plotted using error bar in each setting, shown in figure.

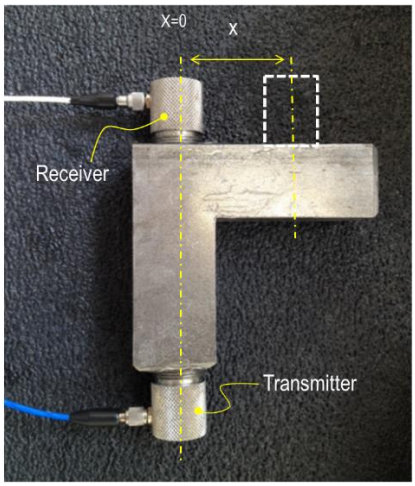

Figure 4-12: Face-to-face transmission set up in angled structure

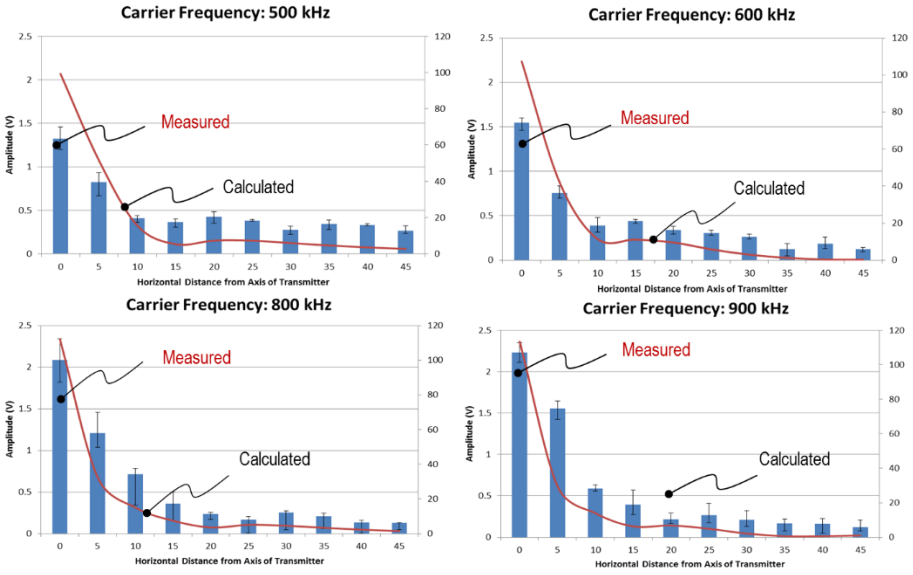

Figure 4-13: Calculated and measured signal strength (Unit of lateral position, *x: mm*)

As the horizontal distance (*x: mm*) increases, the received signal amplitude decreases due to the concentrated signal on the axial axis of the transmitter. As the carrier frequency increases, it is seen that the received signal strength increase in near field, between 0 – 10 mm, while shows a decay during the far field, between 25 – 40 mm. Thus suitable placement of receiver is critical for face-to-face transmission in angled structure. For example, a low carrier frequency is feasible for non-aligned transmission in far field.

Figure 4-14 (a) shows the details of experimental set up during the end-to-end transmission in angled structure, the same as that of last experiment. During this experiments, 500 kHz, 600 kHz, 700 kHz, 800 kHz, 900 kHz are used as the carrier wave frequencies for acoustic-based data transmission. The red line corresponds to the calculated value from the analytical model, while the mean value during each setting was highlighted in blue bar. Standard deviation is plotted using error bar in the Figure 4-13 (b).

Specially, for such case, signal strength is determined by the structure of side lobes. Optimal frequency at 600 kHz can be estimated from theoretical model confirmed by the experimental results.

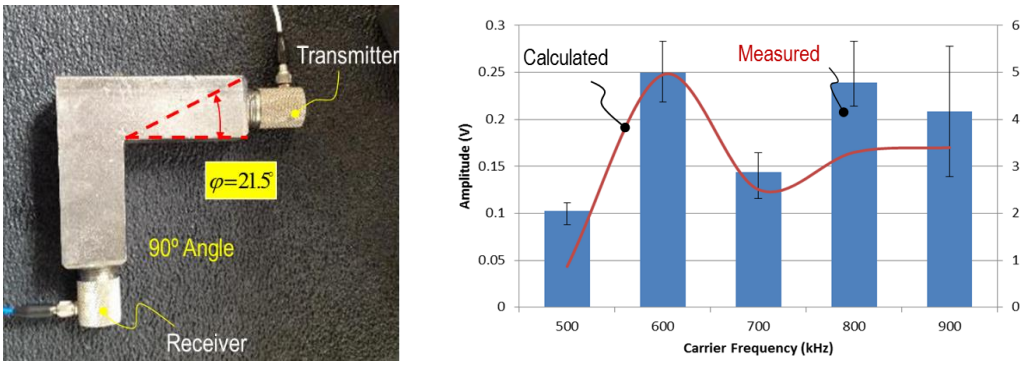

(a) Experimental set up (b) Experimental results

Figure 4-14: End-to-end transmission in angled structure

4.5 Summary

Acoustic wave propagation in a metallic structure was analytically and experimentally evaluated to quantify the effect of several parameters that have impact on the accuracy and reliability of acoustic wave based signal transmission, including transmission distance, carrier frequency, and transmitter–receiver misalignment. Some representative structures are designed and prototyped for study of the effect of placement of receiver and transmitter on the accuracy of acoustic-based data transmission. Good correlation

between the theoretical model predication and experimental observation across a range of frequencies and misalignment has been confirmed. The modulated sensor signal can be successfully received and extracted from the acoustic wave when the misalignment between the transmitter and receiver is less than an angular displacement of approximately 14 °.

High data transmission rates and low bit error rates can best be achieved when the receiver is within the main lobe of the transmitter wave during the face-to-face transmission in rectangular metal plate. While the feasible placement for receiver during the face-to-face transmission in angled structure, could be determined by both the carrier frequency and misalignment. The feasible carrier frequency used in the end-to-end transmission in angled structure is selected through the structure of side and main lobe. As implemented, an 8-bit signal was encoded in a modulated signal having a frequency of 1.4 MHz and duration 0.1 ms. This paradigm is sufficient for data transmission at rates of 10 kbps. Given the high speed of sound and low attenuation in metallic structures, acoustic-based data transmission is a viable technique for embedded wireless sensing in industrial applications.

CHAPTER 5

ONLINE PRODUCT QUALITY MONITORING

5.1 Overview

Quality is a determining factor that affects the productivity and economy of production, especially in the case of mass production. Traditionally, quality control is performed offline, after a part is produced, by measuring the quality attributes either for all the parts or a select batch, based on statistical analysis to ensure that a pre-defined probability of quality production is achieved [74]. Advancement in sensing technology over the past decade has made it possible to directly measure or infer the quality of product during some manufacturing processes. Vibration measurement has been performed during milling process to detect chatter, which affects part quality [75]. Surface finish quantification at the scale of 10-100 *nm* has been performed for fatigue life estimation [76] of hard turned and ground surfaces. Similar quality measurement techniques have also been applied to sanding and milling, using acoustic and strain sensors [77].

Compared to machining and additive manufacturing, net-shape manufacturing processes such as moulding, extrusion, and stamping typically provide significant material and processing cost advantages. In net-shape manufacturing processes, products are formed directly from constitutive materials without the need for subsequent processing. However, a fundamental difficulty in such processes is that few of the product properties can be ascertained *in situ*. Furthermore, quality attributes (such as part dimensions) are often sensitive to variations in process states (such as temperature and pressure). For these reasons, net-shape manufacturing of precision components has remained challenging even with advances in instrumentation technology and machine designs. One example is plastic moulding where the melt plastic is injected into an enclosed metal cavity with high pressure and temperature to form the desired geometry after cooling and solidification. In injection moulding, industry standards for tight tolerances are specified as maintaining dimensional variances within 0.1% of the nominal length, sometimes with dimensional

tolerances at the μm-level [78]. Such tight tolerances may be required for locating optical or electrical parts and ensuring reliable structural performance [79].

Although the initial pressure and temperature of the polymer melt are set and controlled by the machine, the actual melt states (pressure, temperature, velocity, and viscosity, as shown in Fig. 5-1) varies in the mould cavity with other environmental parameters (e.g., residual temperature distribution in the mould cavity), resulting in the part dimension variations of the final product. To obtain the desired critical-to-quality attributes (CTQs) of precision manufactured products, processes and instrumentation must be consciously designed such that the key process variables (KPVs) are observable and controllable. Failure to understand and control the linkage between KPVs and CTQs may result in undesirable levels of defects during production, unattained levels of specified precision, and technical and/or economic infeasibility of the intended application [80]. Prior research [81] has found in blind validation trials that trade-offs exist between acceptance of defective products and unnecessary rejection of acceptable products. The goal of this research is to develop a quality control system that can predict product quality to an accuracy of 3 errors per million opportunities as specified by six sigma methodologies to ultimately enable fully automatic, high quality production.

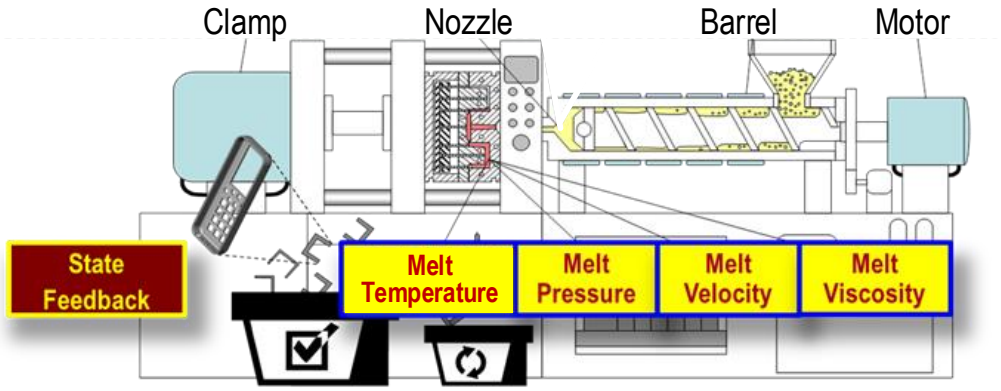

Figure 5-1: Process parameters affecting part quality in injection molding

Towards this goal, this chapter presents an in-process measurement technique for monitoring the quality of injection moulded parts, based on the hypothesis that quality metrics, such as the part's thickness and width, can be tightly controlled if key states of the process are known *in-situ*. To quantify the process states,

a custom-designed multivariate sensor (MVS) is embedded into the mould cavity of a commercial, all-electric injection moulding machine. The sensor measures two parameters of the melt (pressure and temperature) when the polymer melt is injected into the cavity, and infers another two parameters (velocity and viscosity) through mechanistic relations [71]. Process features affecting part quality (e.g., maximum value of measured parameters) are extracted from the raw signals to train a model that correlates newly moulded parts with new sensor data, and predicts part dimensions in future production runs.

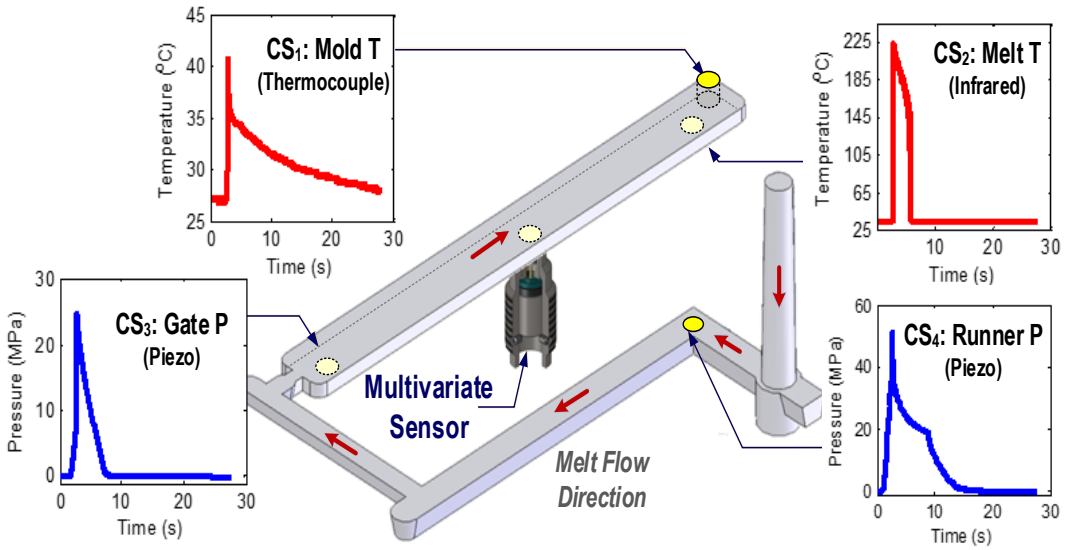

Figure 5-2: Process instrumentation using commercial sensors and multivariate sensor

5.2 Process Instrumentation

The geometry of the instrumented mould cavity in a production grade injection moulding machine is illustrated in Figure 5-2 by the moulded part, which is a flexure bar for experimental tests according to the ASTM (American Society for Testing and Materials) standard. The mould has two piezoelectric pressure sensors (Priamus 6001A) built into its structure, near the entrance to the runner system and gate to the cavity, respectively. An in-mould thermocouple (Priamus 4001A) and an infrared melt pyrometer (Omega OS1562) are located at the end of the melt flow. In addition, a thermopile (Heimann HMSZ11-F5.5) is placed at the end of the cavity for infrared detection due to its good responsivity across the wavelength range (4.8-9.7 μm) of this study, together with a thermistor for mould temperature sensing.

Figure 5-3 illustrates the working principle of the MVS sensor, which is placed at the mid-point of the cavity between the gate pressure sensor (CS_3) and melt temperature sensor (CS_2).

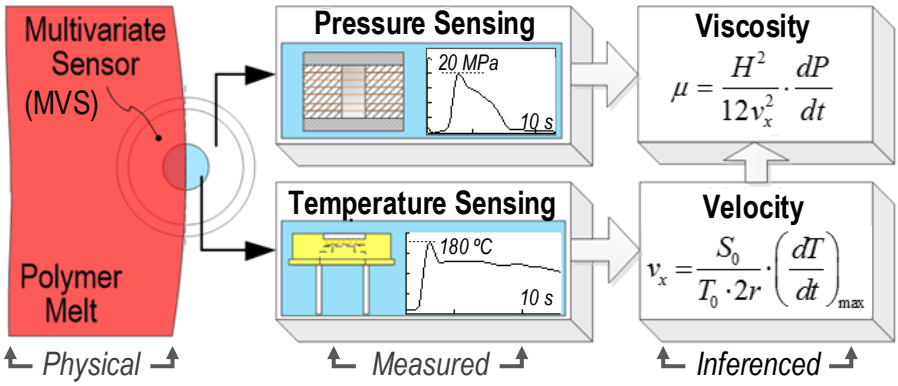

Figure 5-3: Multivariate sensor working principle

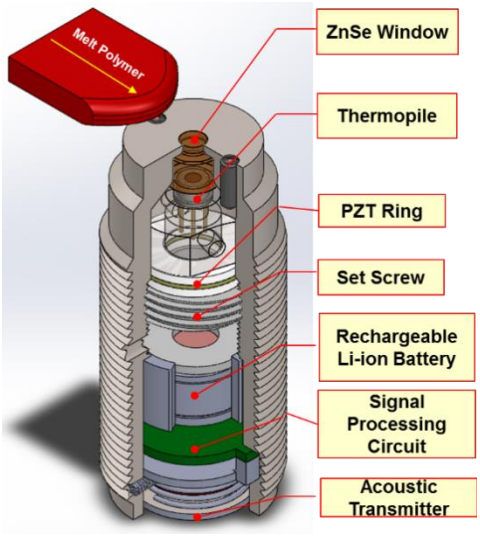

Figure 5-4: Overview of multivariate sensor

The MVS in Figure 5-4 incorporates a PZT ring (0.5 mm thickness with an inner and outer diameter of 3.5 and 6.0 mm, respectively) located behind a metal stand-off. A thermopile, set behind a cylindrical glass window at the top of the MVS package, measures the melt temperature by converting infrared (IR) radiation from the melt into a proportional voltage signal as it flows across the window. Since the incident radiative power is proportional to the area of the polymer melt as it crosses the lens, the velocity of the melt front

can be inferred by taking the maximum rate of sensed temperature increase during the injection of the polymer melt as:

$$v_x = [S_0 / (T_0 \cdot 2r)] \cdot (dT / dt)_{\max} \tag{5-1}$$

where T_0 is the peak melt temperature measured by the thermopile, and S_0 and r are the footprint area and radius of the lens, respectively. Assuming viscous flow, the viscosity of melt is inferred from the pressure ramping rate and melt velocity as:

$$\mu = (H^2 / 12 v_x^2) \cdot dP / dt \tag{5-2}$$

where H is the height of the mould cavity, and v and dP/dt are the melt front velocity and time rate of pressure change, respectively.

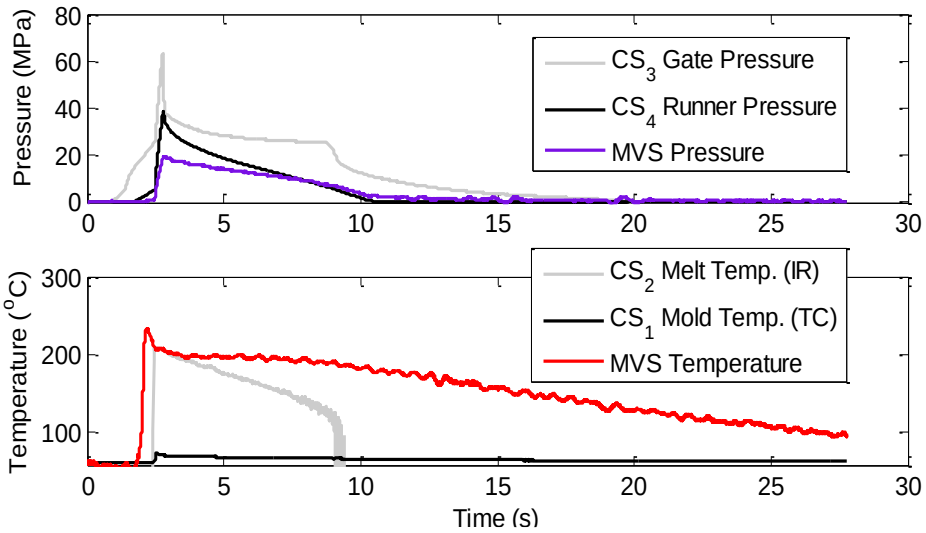

Figure 5-5: Process states for one sample molding cycle

The process states measured by the commercial sensors and MVS are shown in Fig. 5-5 for a representative moulding cycle in a Design of Experiments (DOE). The upper plot indicates that the injected melt first reaches the runner pressure sensor, then the gate pressure sensor, and finally the MVS, consistent with their respective locations. There is a pressure drop between each sensor associated with the viscosity of the melt and its flow resistance. Comparing the melt temperature measured by the MVS to that of the

commercial pyrometer (CS_2) in the lower plot of Fig. 5-5, it is seen that the MVS detected the arrival of the melt before CS_2, and with a slightly higher reading. This is because CS_2 has a minimum temperature of 80 °C and thus clips the process data at the start and end of its readings. By comparison, the MVS admits a wide wavelength range and captures a more complex temperature behaviour, including the cooling of the melt in the mould cavity. The otherwise good agreement between MVS and the commercial sensor validates the functionality of the MVS.

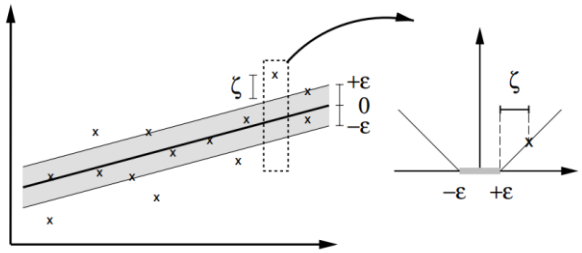

Figure 5-6: The soft margin loss setting in SVR

5.3 System Modelling

5.3.1 SVR framework

The measurement sensor data sets $\{(\boldsymbol{x_1}, \boldsymbol{y_1}), \ldots, (\boldsymbol{x_l}, \boldsymbol{y_l})\} \subset \boldsymbol{\mathcal{X}} \times \mathbb{R}$, where $\boldsymbol{\mathcal{X}}$ denotes the space of the input patterns ($\boldsymbol{\mathcal{X}} = \mathbb{R}^{\boldsymbol{d}}$). Our goal is to find a function $\boldsymbol{f(x)}$ that has at most $\boldsymbol{\varepsilon}$ deviation from the actually obtained targets $\boldsymbol{y_i}$, for all the training data, and at the same time is as flat as possible. In other words, we do not care about errors as long as they are less than $\boldsymbol{\varepsilon}$, but will not accept any deviation larger than this. This may be important if we want to be sure not to lose more than $\boldsymbol{\varepsilon}$ accuracy when doing the online product quality predication.

For pedagogical reasons, we begin by describing the case of linear function $\boldsymbol{f}$, taking the form

$$f(x) = \langle \omega, x \rangle + b \;\; with\; \omega \in \mathcal{X}, b \in \mathbb{R} \tag{5-3}$$

where $\langle \cdot, \cdot \rangle$ denotes the dot product in $\boldsymbol{\mathcal{X}}$. Flatness in the case of (5-3) means that on seeks a small $\boldsymbol{\omega}$. One way to ensure this is to minimize the norm, i.e. $\|\boldsymbol{\omega}\|^2 = \langle \boldsymbol{\omega}, \boldsymbol{\omega} \rangle$. One drawback of such a regression boundary function built in the original feature space is that it is often times a complex, nonlinear, and implicit function which is computational demanding for predicating injected product quality for each new data point added. To overcome this limitation, the part quality are assumed to be predictable in an enlarged feature space with higher dimensionality than the original feature space. To achieve this, the SVR algorithm first transforms the data $\{\boldsymbol{x_i}\}$ from the original lower dimensional space to a higher-dimensional space via a transformation function $\boldsymbol{\phi}(\boldsymbol{x})$. A hyper-plane $\boldsymbol{f}(\boldsymbol{x}) = \boldsymbol{\omega^T \phi}(\boldsymbol{x}) + \boldsymbol{b}$, is then built in the higher-dimensional space to predict the part quality (part's dimension: thickness or width). In this formulation, $\boldsymbol{\omega}$ and $\boldsymbol{b}$ are the weighing factors and $\boldsymbol{\phi}(\boldsymbol{x})$ is the transformed data set in high dimension [82]. To allow for some prediction error during the practical application, analogously to the "soft margin" loss function, one can introduce slack variable $\boldsymbol{\xi_i}$, $\boldsymbol{\xi_i^*}$ to cope with otherwise infeasible constraints of the optimization problem. Thus, we can write this problem as a convex optimization problem:

$$\begin{aligned} &minimize \quad \frac{1}{2}\|\omega\|^2 + C\sum_{i=1}^{\ell}(\xi_i + \xi_i^*) \\ &subject\ to \quad \begin{cases} y_i - \langle \omega, \phi(x) \rangle - b \ \leq \ \varepsilon + \xi_i \\ \langle \omega, \phi(x) \rangle + b - y_i \ \leq \ \varepsilon + \xi_i^* \\ \xi_i, \xi_i^* \ \geq \ 0 \end{cases} \end{aligned} \tag{5-4}$$

The constant $\boldsymbol{C > 0}$ determines the trade-off between the flatness of $\boldsymbol{f}$ and the amount up to which deviations larger than $\boldsymbol{\varepsilon}$ are tolerated. This corresponds to dealing with a so called $\boldsymbol{\varepsilon}$-insensitive loss function $|\boldsymbol{\xi}|_{\boldsymbol{\varepsilon}}$ described by

$$|\boldsymbol{\xi}|_{\boldsymbol{\varepsilon}} = \begin{cases} 0 & if\,|\xi| \leq \varepsilon \\ |\xi| - \varepsilon & otherwise \end{cases} \tag{5-5}$$

Figure 5-6 illustrates the situation graphically. Only the points outside the shaded region contribute to the cost insofar, as the deviations are penalized in a linear fashion. Utilizing Lagrange multipliers, we could establish a standard dualization method to convert it into dual formulation with the saddle point.

$$maximize \quad \begin{cases} -\frac{1}{2}\sum_{i,j=1}^{\ell}(\alpha_i - \alpha_i^*)(\alpha_j - \alpha_j^*)\langle\phi(x_i), \phi(x_j)\rangle \\ -\varepsilon\sum_{i=1}^{\ell}(\alpha_i + \alpha_i^*) + \sum_{i=1}^{\ell} y_i(\alpha_i + \alpha_i^*) \end{cases} \tag{5-6}$$

$$subject\ to \quad \sum_{i=1}^{\ell}(\alpha_i - \alpha_i^*) = 0\ and\ \alpha_i, \alpha_i^* \in [0, C]$$

where $\boldsymbol{\alpha_i, \alpha_i^*}$ are Lagrange multipliers. Thus we could solved as follows [83]:

$$f(x) = \sum_{i=1}^{\ell}(\alpha_i - \alpha_i^*)\langle\phi(x_i), \phi(x)\rangle + \mathrm{b} \tag{5-7}$$

Compared with Eq. (5-3), we know that $\boldsymbol{\omega = \sum_{i=1}^{\ell}(\alpha_i - \alpha_i^*)\phi(x_i)}$. It is seen that the decision function can be determined without specifying the explicit form of the transformation $\boldsymbol{\phi}$, but only the kernel function $\boldsymbol{K(x_i, x) = \langle\phi(x_i), \phi(x)\rangle}$ that computes inner products. Replacing the inner product in Eq. (5-7), the regression function for part quality prediction can be rewritten as:

$$f(x) = \sum_{i=1}^{\ell}(\alpha_i - \alpha_i^*)K(x_i, x) + \mathrm{b} \tag{5-8}$$

For the present study, the polynomial kernel was selected due to its reported effectiveness in regression model.

5.3.2 Feature extraction and SVR based quality estimation

In this quality control technique, the model relating the MVS outputs to the moulded part quality attributes is first established with characterization experiments. Subsequently, the validated model is applied continuously to predict the width and thickness of new moulded parts with real-time sensor data in lieu of intermittent quality acceptance sampling. While this approach requires model development and validation on an application-specific basis, net-shape manufacturing applications have long production runs and the benefits associated with higher quality assurance and more timely feedback of production defects far outweigh the costs of the initial training. In particular, this approach is highly warranted for injection moulding, wherein the thermal expansion and compressibility behavior of the melt directly governs the final product dimension while requiring long time periods (e.g., days) for the dimensions to equilibrate.

Due to the nonlinear and non-uniform temperature and pressure distributions in the mould cavity, it is generally difficult to establish an accurate physical model that relates the mould/melt characteristics to part dimension in real-world operations. To quantify such a relationship, a data-driven model based on the support vector regression (SVR) algorithm has been developed. The model estimates the correlation between the features extracted from sensor data obtained through in-process measurement and associated part dimensions measured off-line. It also minimizes the total error bound for achieving global minima of the error between the predicted and measured part dimensions. It is noted that some of the features extracted from the moulding processes are not absolutely independent from each other. For example, although the melt pressure is primarily determined by the packing pressure setting of the machine, it may change rapidly in the cavity if the temperature decreases. The SVR-model is able to differentiate the various input characteristics while maintaining the estimation accuracy.

To correlate part quality with process measurement, features have been extracted from the raw sensor data. An example of the extracted features is shown in Fig. 5-6:

1) Peak values of the pressure and temperature as the melt flows across the MVS, which describe the physical state of the melt such as thermal expansion and volumetric change during the fluid-solid transition;

2) Melt velocity, calculated from the maximum temperature ramping rate *dT/dt* (Eq. 5-1) which describes the flow of the melt within the mould cavity as the melt is injected into it;

3) Melt viscosity, calculated from the pressure ramping rate *dP/dt* (Eq. 5-2), which determines the flow behaviour of the melt that in turn affects the geometry/dimension of the moulded part;

4) Cooling rate of the melt, which indicates the rate of part cooling during the solidification process. Variation in the rate affects part shrinking and consequently, part dimension.

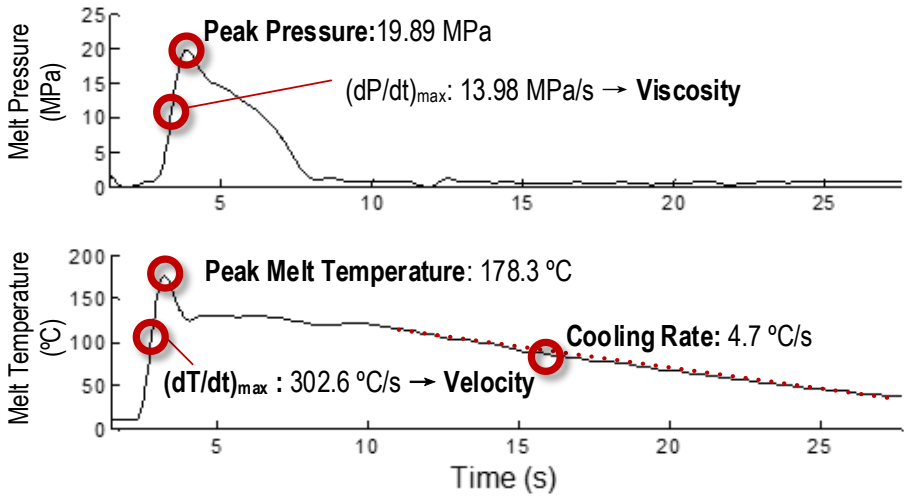

Figure 5-6: Features extracted from the MVS

From the commercial sensors, features extracted include the peak pressure at the runner and gate, peak temperature and cooling rate at the end of the cavity (see Fig. 5-2). The SVR-based quality estimation model involves two interrelated operations. First, the model extracts features from the historical data and fuse them to establish the correlation function toward the offline measured part dimension. Assume a dataset $\{\boldsymbol{x}_i\}$ is established that contains features measured by MVS and/or the commercial sensors, where $i = 1, 2, \ldots N$ (N: total number of training cycles) and each vector $\boldsymbol{x}_i$ contains five features as specified in Fig. 5-6. The model finds the predicted dimension $f(x)$ on a hyper-plane that has the minimal difference from the actual, measured dimension, for all the training data. Such a function $f(x)$ can be expressed as:

$$f(x) = \omega^T \phi(x_i) + b \tag{5-9}$$

where ω and b are the weighting factors obtained through the training process, and $\phi(\boldsymbol{x}_i)$ is the transformation function converting $\{\boldsymbol{x}_i\}$ from the low-dimensional space to a higher-dimensional space. In the second operation after the training procedure, the established relationship is applied to estimating the actual part dimension in real moulding process by substituing the measured features, such as $\boldsymbol{x}_i$, in Eq (5-3).

5.4 Experimental Evaluation and Data Analysis

To evaluate the developed part quality prediction method, an MVS sensor was prototyped and tested on a commercial injection moulding machine (model SD750UZ), as shown in Fig. 5-7. The cavity contains a piezoelectric pressure transducer (Priamus 6001A, Schaffhausen, Switzerland) near the gate. At the end of the cavity there is an exposed type-N thermocouple (Primaus 4001A) as well as an infrared melt pyrometer (Omega OS1562, Stamford, CT). The MVS was installed at the center of the cavity. This mold was installed on a fully electric injection molding machine (Sumitomo SE75DUZ). Four machine signals, including; injection pressure, screw position, linear screw velocity, and screw rotational speed (RPM), as well as data from the commercial sensors were acquired via a Priamus eDAQ 8102A at 500 Hz. Data from the MVS was acquired by a National Instruments X6351 at a rate of 10 kHz.

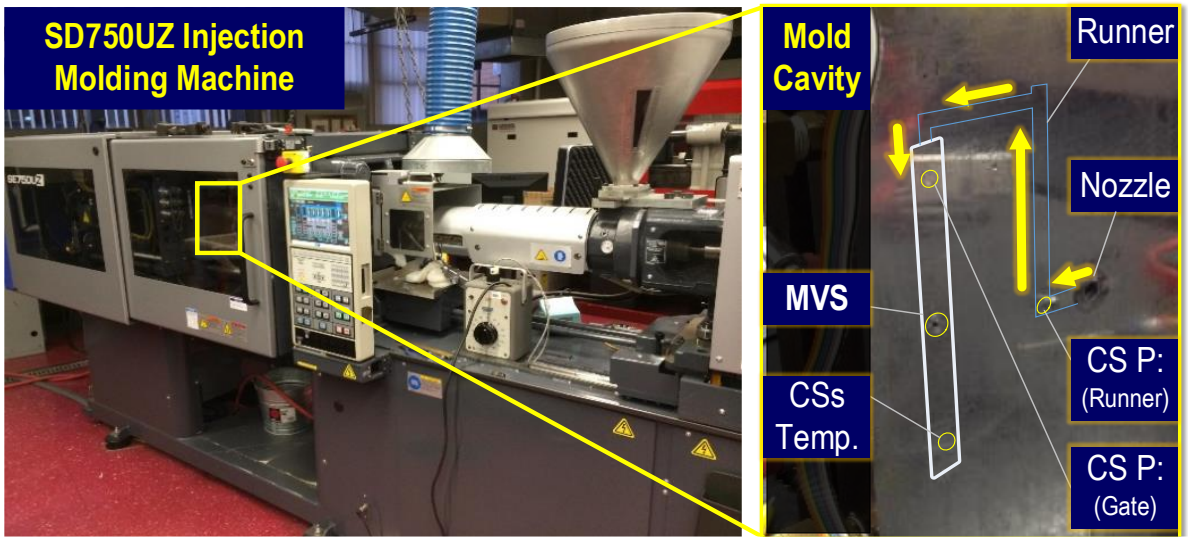

Figure 5-7: Experimental setup

A Design of Experiments (DOE) was performed to characterize the behavior of the moulded part dimension to the process settings. Specifically, a half fractional factorial design for melt temperature, mould coolant temperature, and packing pressure was replicated for three different injection velocities. This design yielded $2^{3-1} \cdot 3 = 12$ runs. The polymer resin was high impact polystyrene (HIPS, Dow Styron 478). During experimentation, time is allowed for the machine to reach the set points for the melt and mold temperature.

The injection molding machine is then operated for fifteen minutes before collecting samples to ensure the process reached steady-state. In Table 1, the DOE machine settings and part thickness statistics are shown.

Table 5-1: Design of experiments, factors, and results

Run	T_{melt} ***(°C)***	T_{mold} ***(°C)***	P_{pack} ***(MPa)***	V_{inject} ***(mm/s)***
1	190	21	30	10
2	190	21	30	40
3	190	21	30	100
4	190	60	50	10
5	190	60	50	40
6	190	60	50	100
7	220	60	30	10
8	220	60	30	40
9	220	60	30	100
10	220	21	50	10
11	220	21	50	40
12	220	21	50	100

Each of the DOE run settings was replicated 20 times. Data measured in the first 15 cycles were used for training the part dimension-prediction algorithm while data from the remaining five cycles were used for validation. To measure the dimension of the moulded part, a test rig was designed and prototyped, which can be seen Figure 5-8. The thickness and width of the part were measured by a micrometer at the center point between the MVS and commercial pressure sensor (see Fig. 5-2).

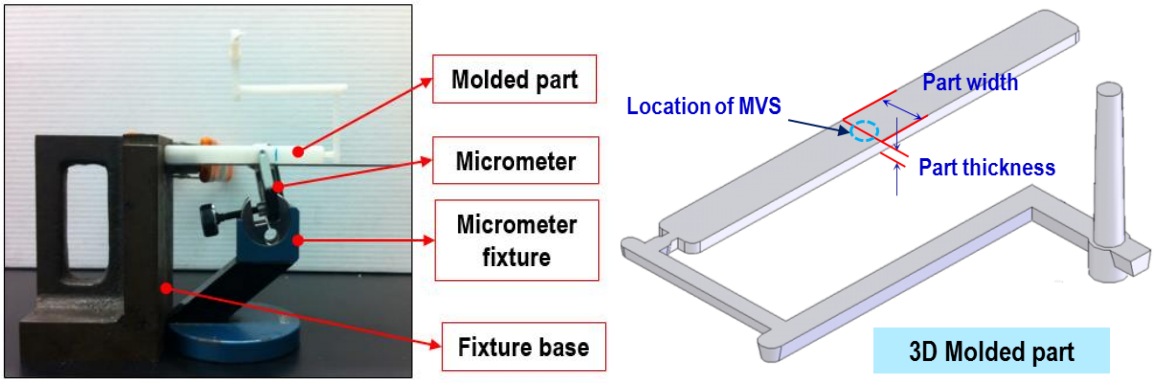

(a) measurement structure (b) 3D product

Figure 5-8: Measurement rig and measurement location

In Figs. 7-8, results of part thickness prediction based on the SVR model are validated using part thickness measurement. Specifically, Fig. 7 shows the correlation between the predicted and observed part

thicknesses using data from the MVS sensor (yellow square) and commercial sensors (blue diamond), respectively. The diagonal represents the ideal case, with data points located near the diagonal having smaller prediction errors. To restrict the comparison to the sensors only, no machine setting data were included in the result.

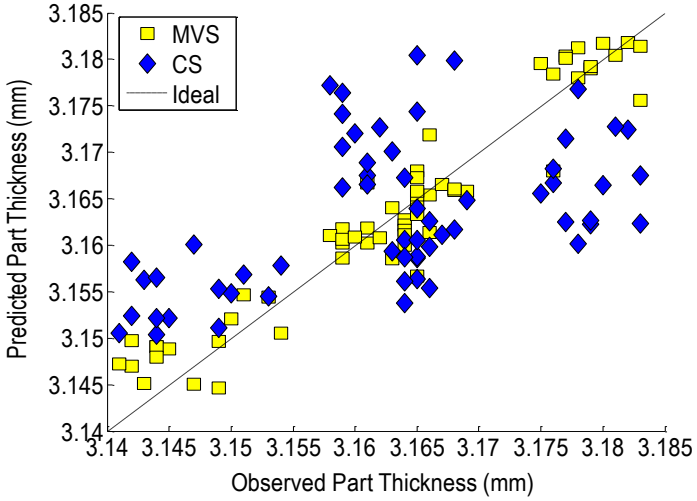

Figure 5-9: Thickness prediction w/o machine settings

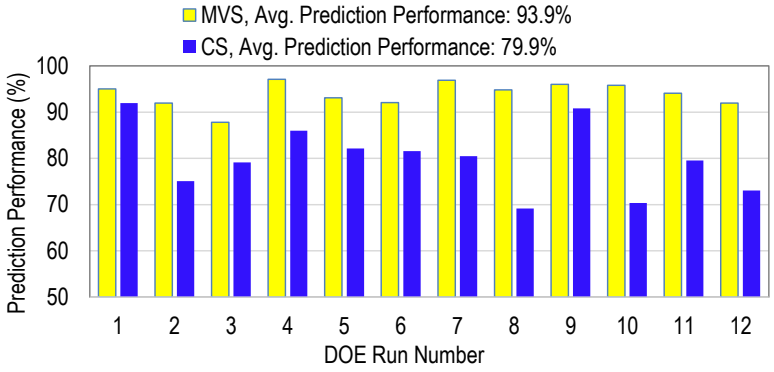

Figure 5-10: Performance of thickness prediction w/o machine settings

Figure 8 shows the performance comparison of thickness prediction by the MVS and commercial sensors. It is seen that MVS outperformed CS in all the DOE runs, with the prediction accuracy equal 93.9%, compared to 79.9% by CS. The result is of significance, in that the single MVS replaces a total of four commercial sensors installed at three different locations across the mould cavity. The improved sensing performance results not from the placement of the sensor but rather the mechanistic analysis of the

acquired sensing schemes to estimate the velocity and viscosity, thereby providing additional information as to the state of the material being moulded.

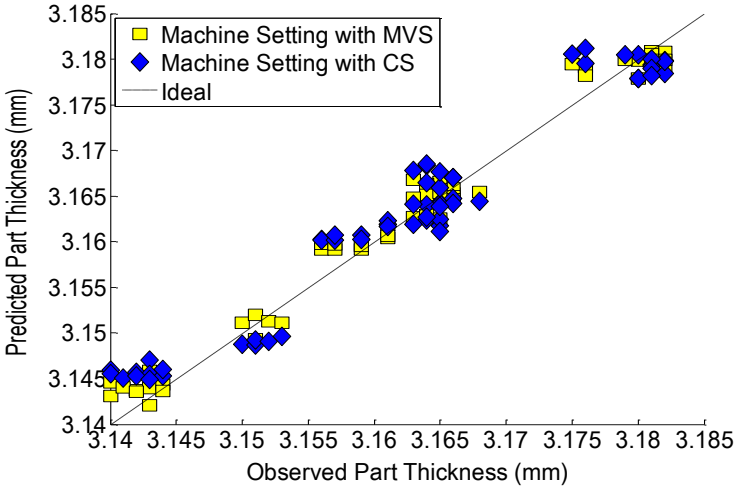

Figure 5-11: Thickness prediction with machine settings

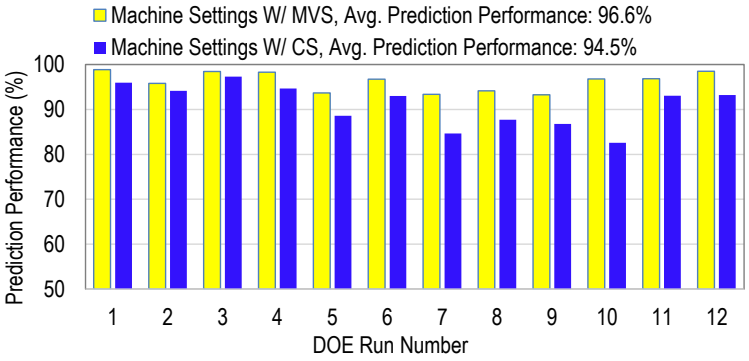

Figure 5-12: Performance of thickness prediction with machine settings

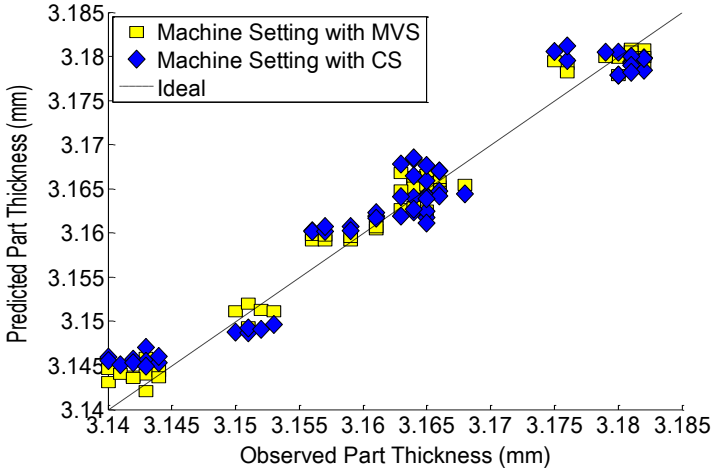

Figure 5-13: Width prediction w/o machine settings

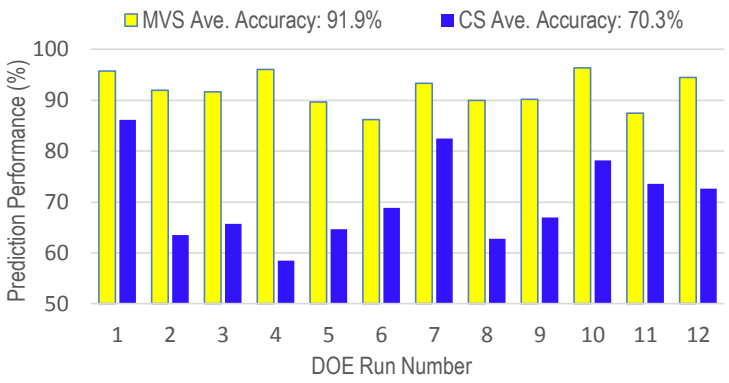

Figure 5-14: Performance of width prediction w/o machine settings

Figures 9 and 10 illustrate the results when machine settings, as represented in the first four columns of Table 1, were added as additional input $\boldsymbol{x}_i$ to train the SVR-prediction model. Because these parameters govern the input state of the polymer melt, they have a significant effect on the final part quality. However, it is the local state of the polymer melt in the mould cavity that determines the final product quality [84]. As such, the MVS' increased responsiveness and more advanced analysis of the process states has led to an overall improvement in the part quality prediction, as indicated by the closeness of the data points to the ideal case scenario. Specifically, the average performance of part thickness prediction using commercial sensors combined with machine setting has improved to 94.5%, whereas with MVS, it is 96.7%. This again verifies that MVS has performed better, in every one of the 12 DOE runs.

Similar analysis has been performed for predicting the part width. As summarized in Table 2, high correlation between the in-process measurement and part dimension (thickness and width) has been achieved. Using four parameters measured or inferred by the MVS sensor, coefficient of determination (R^2) greater than 95% has been achieved, which is significantly higher than using the commercial sensors, due to the increased amount of information incorporated in the SVR-model.

Furthermore, prediction using MVS sensor also has shown to have improved the robustness, as indicated by the lower standard deviations when compared with the result from commercial sensors, for all the part thickness and width predictions, with or without including machine settings. This confirms the hypothesis that in-process measurement provides an effective tool for online part quality monitoring. From a

mechanistic viewpoint, the presented technique demonstrates high predictive capability because the empirical model reflects the underlying physics. Specifically, the thermal expansion and compressibility behavior of the material being formed directly governs the final product dimensions in injection moulding. This behavior is well-represented by constitutive models such as the double domain Tait equation, which presents the specific volume, *v*, as a function of the melt's pressure and temperature [85].

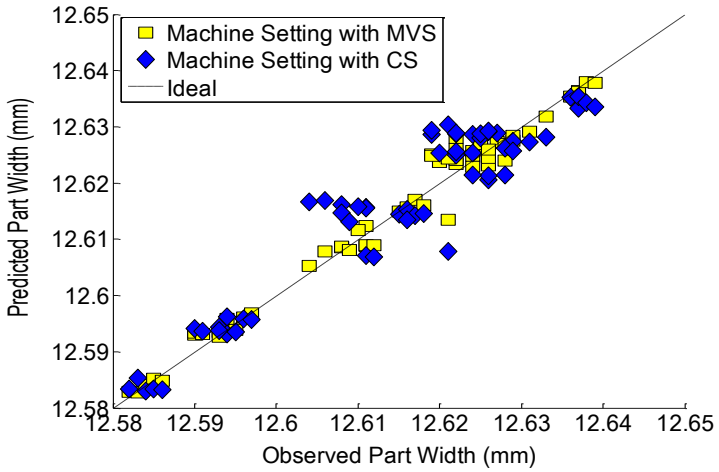

Figure 5-15: Width prediction with machine settings

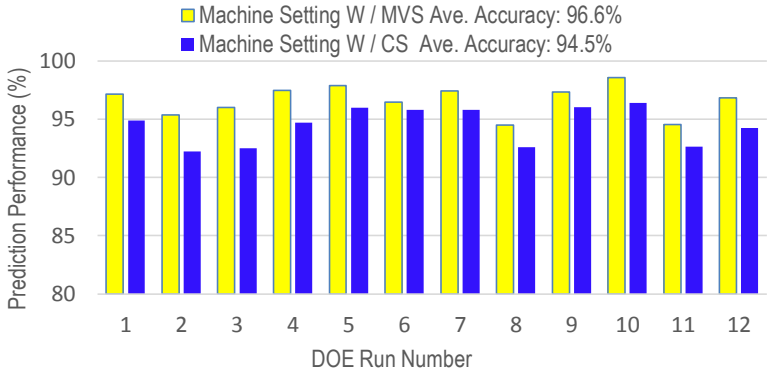

Figure 5-16: Performance of width prediction with machine settings

The developed SVR model, in effect, derives suitable coefficients that reflect the physics of the process. The results of Table 2 suggest that higher fidelity models can be obtained by using multiple sensor streams such as pressure, temperature, velocity, and viscosity that are indicative of different states of the product being formed. While the models could be derived *a priori* from the product/tool design and characterized

material properties, uncertainty in material characterization, boundary conditions, and geometry in practice will necessitate verification on an application-specific basis, which motivates the presented technique.

Table 5-2: Performance of prediction for thickness and width

	Input Data Type	R^2 (%)	Min (%)	Max (%)	Std. Dev	Avg. (%)	Difference(%)
Thickness Estimation	CS	46.0	54.1	97.6	10.7	79.9	*13.9*
	MVS	95.6	81.5	99.9	4.8	93.9	
	Machine	96.4	82.3	97.6	3.8	91.5	*3.0*
	CS + Machine	98.0	86.7	99.9	3.2	94.5	
	MVS + Machine	98.3	89.7	99.8	2.5	96.7	*2.2*
Width Estimation	CS	71.1	46.4	93.7	11.7	70.3	*21.6*
	MVS	95.0	74.7	99.9	5.9	91.9	
	Machine	94.4	76.0	97.1	5.1	88.6	*2.4*
	CS + Machine	97.2	70.8	99.8	6.6	91.0	
	MVS + Machine	98.4	83.2	99.9	3.6	96.2	*5.2*

5.5 Summary

This chapter presents an online product quality monitoring technique, using injection moulding as an example. The technique is based on in-process measurement of four process parameters, enabled by a custom-designed multivariate sensor (MVS) embedded within the mould cavity. A support vector regression model relating the MVS-sensor outputs and part dimensions has been developed, demonstrating an average prediction accuracy better than 93.9 % for part thickness and 91.9% for part width, as confirmed by offline reference measurement using a micrometer. In a broader sense, by estimating intrinsic material properties from multiple sensor streams, application-specific process quality models can be developed with high fidelity to guide process control. Considering the large number of parts produced in a mass production such as injection moulding, sensor-enabled *in-situ* quality monitoring has the potential to significantly improve productivity and quality control while reducing waste, for sustainable manufacturing.

CHAPTER 6

MULTI-SENSOR DATA FUSION FOR MEASUREMENT ACCURACY

6.1 Data Fusion Theory

An ever-increasing interest has been raised in multi-disciplinary research on multisensory data fusion technology, driven by its versatility and diverse areas of application, such as sensor networks, robotics, video and image processing, and intelligent system design. Multi-sensor data fusion is a technology that using synergistic combination of sensory data from multiple sensors to achieve more accurate information than using each individual sensor separately or a single sensor, thus allowing either improved accuracy from existing sensors or the same performance from combination of smaller or cheaper sensors [86,87]. Due to the development limitation and perceptive uncertainties of sensors integrated into system, appropriate data fusion approaches play an important role in reducing overall sensory uncertainties and thus increasing the accuracy of system performance. Multi-sensor data fusion could achieve not only enhanced but also complementary perceptions, also provide more timely information via the parallel processing of sensory data. Other advantages of implementation of multi-sensor data fusion are improved detection, confidence, and reliability, as well as reduction in data ambiguity.

Numbers of challenging issues related to multi-sensor data fusion include data imperfection, data correlation, data inconsistency and data disparateness [88], majority of which arise from the sensor inherent uncertainties caused by noises or device imprecision, diversity of the sensor technologies, and nature of the application environment. Data correlation is especially problematic in multi-sensor fusion system. Sensory data correlation could exist in distributed fusion settings, e.g. various sensors distributed in measurement space, or centralized fusion settings, e.g. multivariate sensor installed at single location. If not accounting for sensory data correlations among multiple measurements, the fusion approach may suffer from over confidence in results or unnecessary sensor cost. The strategies of multi-sensor fusion should be able to deal with these data correlation and produce the consistent results efficiently.

Taking injection molding as an example, multiple commercial sensors are distributed installed in the flexure bar cavity for improved observation of polymer processing. Figure 6-1 shows four commercial sensors (CS_i, i=1,2,3,4) are located at runner, gate, near end cavity, and end of cavity for measurements of melt pressure, melt temperature and in-mold temperature. In addition, a developed multivariate sensor is placed in the midpoint of mould cavity with the capability of measuring four key in-process parameters including: melt temperature, melt pressure, melt velocity and melt viscosity. To establish the relationship between sensory data, e.g. melt temperature or melt pressure, and product quality, e.g. thickness or width of the part, data correlation among these sensory measurements should be eliminated before fusion or taken into consideration when fusion. Otherwise, few improvements on the prediction accuracy of part quality will be achieved through multiple sensor integration and fusion, thus bringing unnecessary installation cost into online process monitoring system. For example, measurements from CS_1 and CS_2 are correlated each other, which means that information extracted from each individual sensor are overlapped, thus reducing total information content. If two sensory measurements are highly correlated, there is no need to install another extra one in the mould cavity. Because the same performance can be accomplished with fewer sensors. In general, orthogonality or low correlation among sensory data is necessary for the implementation of a meaningful multi-sensor data fusion.

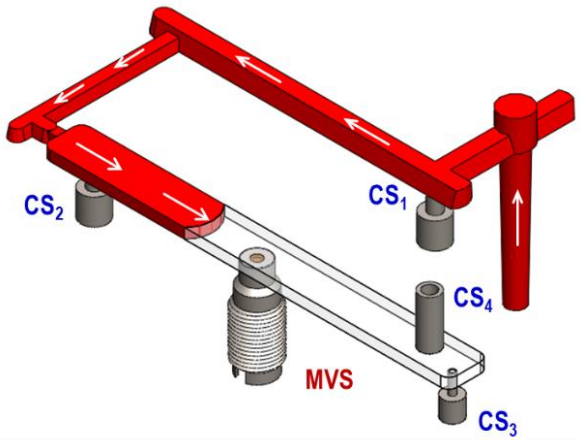

Figure 6-1: Process instrumentation using CS for melt pressure and temperature as well as the developed MVS within an injection mould cavity

6.2 Orthogonality Analysis

A quantification of correlation among sensory data is highly desired for representation of how much two measurements are correlated with each other. Orthogonality analysis based on principle component analysis (PCA) theory [89] is established for evaluating the data correlation. Generally, PCA can be thought of as fitting *n*-dimensional ellipsoid to the data sets, where each axis of the ellipsoid represents a principal component. Small axis of ellipse standing for small variance along that axis can be omitted as well as their corresponding principle components from representation of dataset due to a commensurately small loss on original information. To approximate the information provided by each individual sensor, the first principle vector, along which maximum variance can be achieved for each data point, is selected as an approximated representation of original information for the sensory data. Thus principle angle between any two first principles extracted from sensory data can be an indicator on the correlation of data.

Consider a sensory data set $\{x_i\}$ where $i = 1,2, \dots, N$, and x_i is a D-dimensional vector. Each of the *D* rows represents a set of observations under different machine settings during experiments and each of the *N* columns stands for observations on repetition of experiments. Mathematically, maximum variance of transformed sensory data can be found by projection of sensory data along the first principle axis. The projection is denoted as $y = Ax$, where $A = [u_1^T, \dots, u_M^T]$, $M < D$, and $u_k^T u_k = 1$ for $k = 1,2, \dots, M$. Maximum variance of $\{y_i\}$, which is the trace of the covariance matrix of $\{y_i\}$, is expressed as:

$$A^* = \arg\max tr(\boldsymbol{S_y}) \text{ subject to } \|u\| = 1 \tag{6-1}$$

where

$$\boldsymbol{S_y} = \frac{1}{N}\sum_{i=1}^{N}(y_i - \bar{y})(y_i - \bar{y})^T \tag{6-2}$$

and

$$\bar{y} = \frac{1}{N}\sum_{i=1}^{N} x_i \tag{6-3}$$

Let S_x be the covariance matrix of sensory data $\{x_i\}$. Since $tr(S_y) = tr(AS_xA^T)$, through using Lagrangian multiplier and taking the derivative, we obtain:

$$\boldsymbol{S_x} u_k = \lambda_k u_k \tag{6-4}$$

which means that u_k is an eigenvector of S_x. Thus the first principle axis chosen for the representation of sensory data is the eigenvector of data covariance matrix S_x with the largest eigenvalue.

A Design of Experiments (DOE) was performed to characterize the sensory data correlation from distributed CSs or individual MVS. Specifically, a half fractional factorial design for melt temperature, mould coolant temperature, and packing pressure was replicated for three different injection velocities. This design yielded 12 runs. The details for the DOE machine settings are shown in Table 5-1 in Chapter 5.

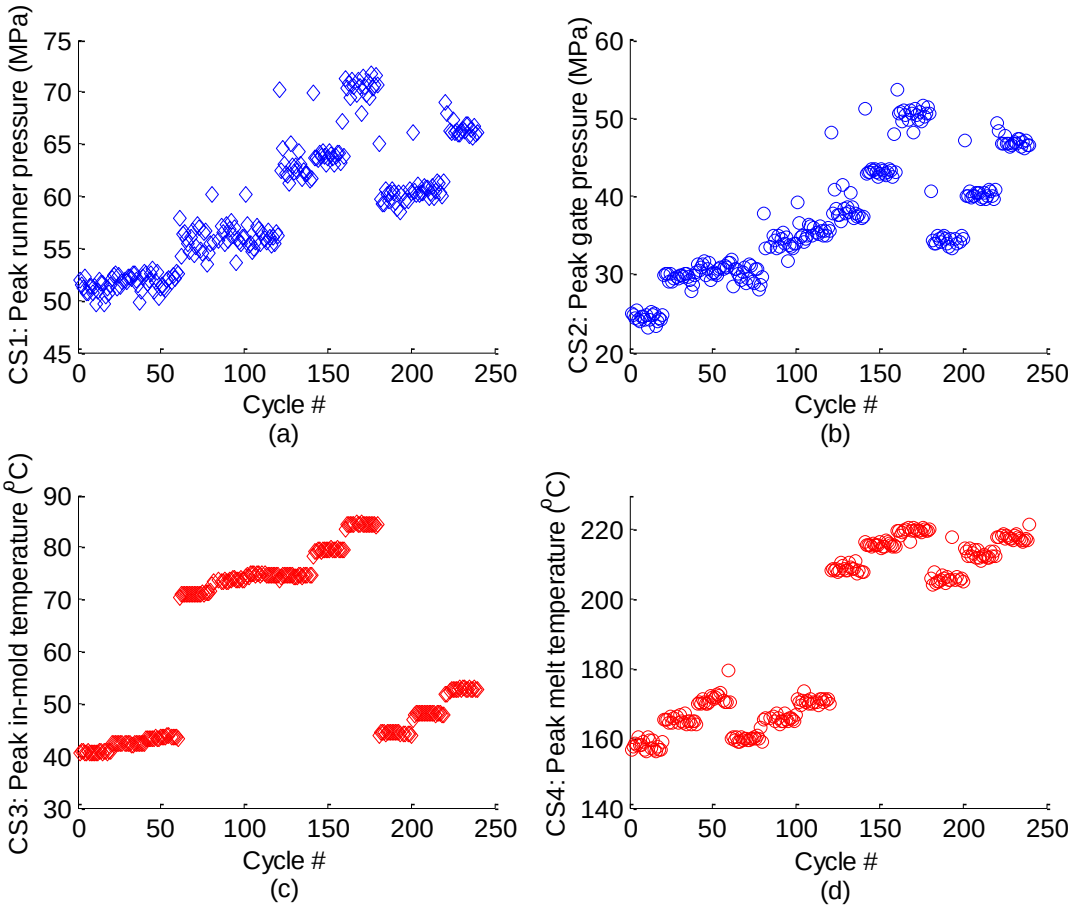

Figure 6-2: Cavity pressures and temperatures from commercial sensors (CS)

Each of the DOE run settings was replicated 20 times. Sensory data from each commercial sensors during each molding cycle are illustrated in Figure 6-2. Specifically, Fig. 6-1, (a) and (b) shows similar variation on peak melt pressure at the runner and gate of mould cavity under different machine settings, as

an indicator of high data correlation. In (c), variation on peak in-mold temperature shows different temperature changes compared with peak melt temperature along the DOE runs, which may cause low correlation between measurements from CS3 and CS4.

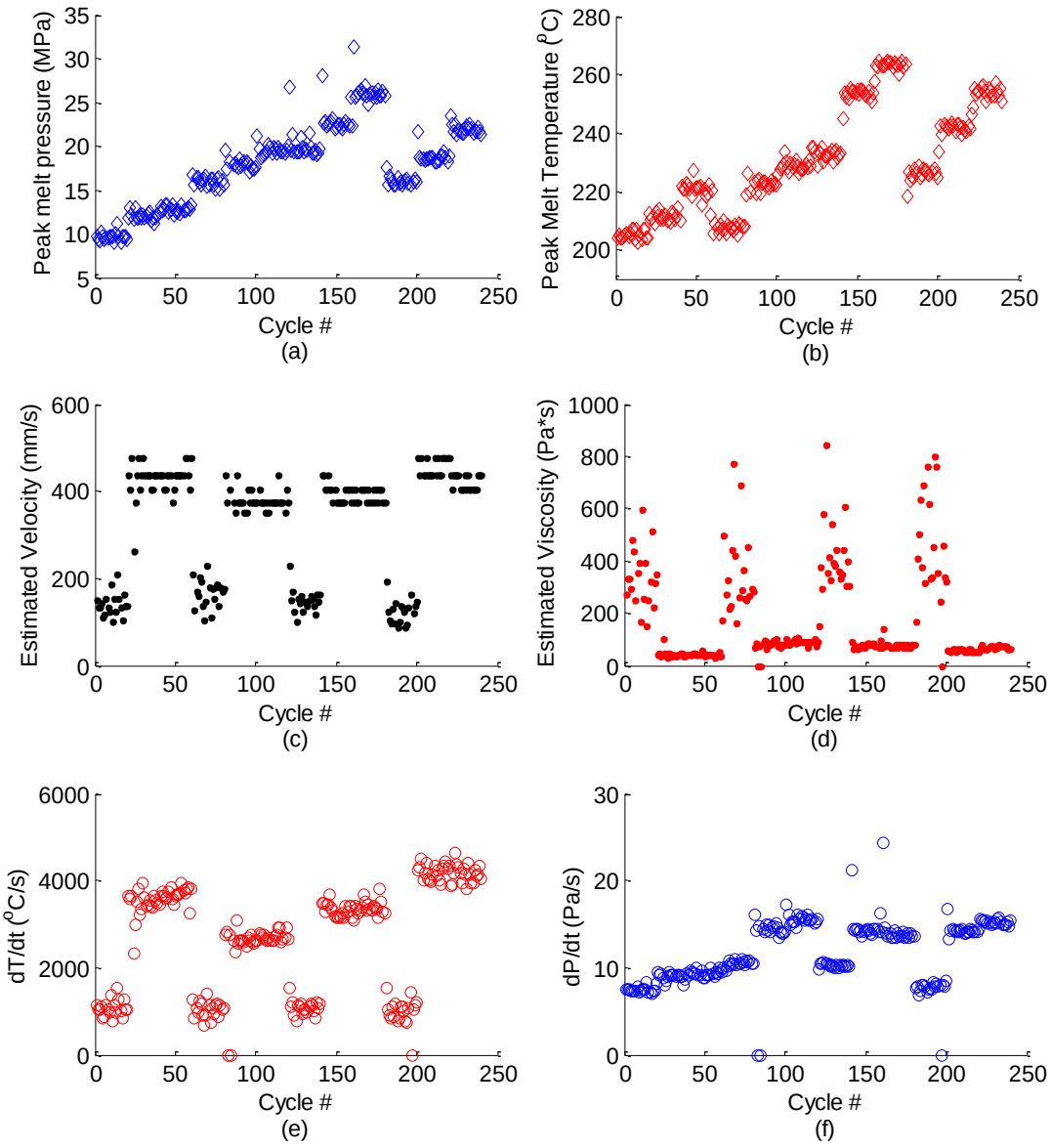

Figure 6-3: Process parameters from multivariate sensor (MVS)

Figure 6-3 shows the raw measurements on different process parameters from one single multivariate sensor located at mid-point of mould cavity. Similar variation can be seen in (a) for peak melt pressure and

(b) for peak melt temperature for the same location when changing the machine settings, indicating that overlapped information may exist between these two sensory data.

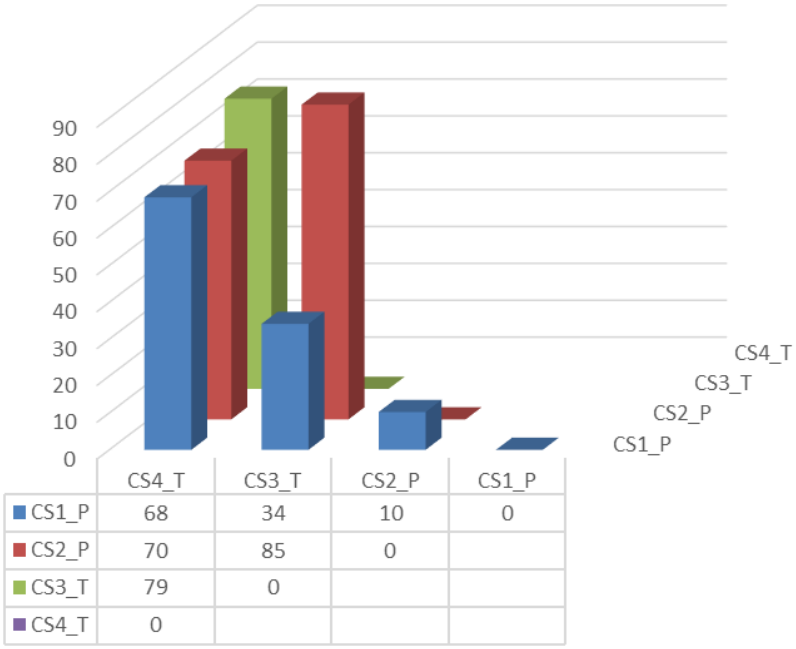

	CS4_T	CS3_T	CS2_P	CS1_P
CS1_P	68	34	10	0
CS2_P	70	85	0	
CS3_T	79	0		
CS4_T	0			

Figure 6-4: Principle angle between CS measurements

To quantify the correlation among sensory data from the polymer processing, the established principle angle method can be calculated from the two first principle vectors and act as a criteria for measuring correlation of data. The more closely the calculated principle angle approaches 90°, the lower correlation exists between these two sensory data sets. A left upper triangle matrix with each individual principle angle between every two commercial sensory data is shown in Figure 6-4. The diagonal value for that matrix are zero showing that two same sensory data sets are totally correlated. Specifically, principle angel between measurements from CS1 for peak runner pressure measurements and CS2 for peak gate pressure measurements is 10°, indicating that high correlation between these sensory data, thus showing a good agreement with the deduction above from Figure 6-2 (a) and (b). During polymer processing, the melt polymer flow through nozzle, runner, gate, midpoint, and to the end of mould cavity, where a closely linear pressure drop exist between each mould section due to Newtonian fluid resistance along the cavity. Thereby, two cavity pressure sensors actually do not provide more process information than a single one does.

The high correlation, indicated as a 79° angel, between measurements from CS3 for measuring in-mold temperature and CS4 show low overlapping in the information space. This occurs due to the larger variation in melt temperature in cavity compared with that in mold temperature in mould plate, which can also be seen from the measurements form Figure 6-2, (c) and (d). High correlation, shown as more than 50° in Figure 6-4, could be found between the measurements from pressure and temperature sensors due to different sensing principles and sensing parameters. In general, more sensors integrated into system don't help much on increasing on the amount of information or improving the observation of polymer processing.

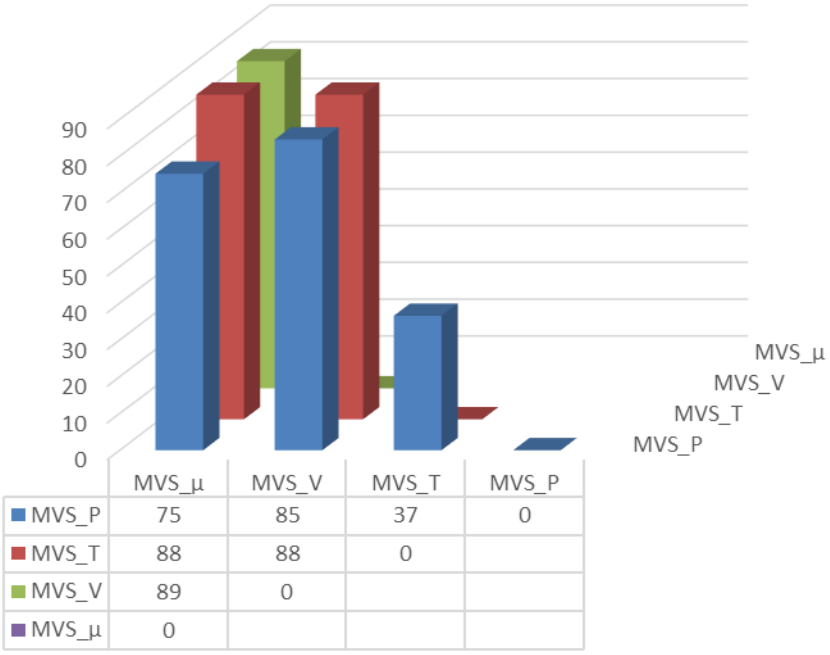

	MVS_μ	MVS_V	MVS_T	MVS_P
MVS_P	75	85	37	0
MVS_T	88	88	0	
MVS_V	89	0		
MVS_μ	0			

Figure 6-5: Principle angle between MVS measurements

Orthogonality analysis is also performed on the four measurements from MVS located at the midpoint of mould cavity. Figure 6-5 shows the principle angles calculated for each two different parameter measurements, e.g. melt velocity to melt viscosity or melt temperature to melt pressure. 37° principle angle between peak melt temperature and pressure shows a certain degree of correlation between these two measurements at the same location, due to similar trend on pressure change and temperature change when adjusting machine settings. Although melt velocity is inferred through maximum temperature ramping rate on melt temperature measurement, large angle 88° implies that these two measurement are almost

orthogonal to each other. It is known that different ramping rate can be derived under different peak melt temperature, which means that inferred velocity is little correlated with melt temperature. From Figure 6-3, it can also be observed that velocity changes a lot while small variation occurs in peak temperature for each three runs. Very low correlation between melt viscosity and melt pressure can be seen in Figure 6-5 with the angle of 75°. This happens to the same reason between the melt velocity and melt temperature. Other principle angles, such as 88° for measurements of melt temperature and melt viscosity, 89° for measurements of melt velocity and melt viscosity, and 85° for measurements of melt velocity and melt pressure, shows that these measurements are almost orthogonal to each other, thereby proving larger amount of information compared with using each individual sensor. Compared with four CSs, much more information are provided by MVS for its low correlations between four parameter measurements.

6.3 Summary

Multi-sensor data fusion enables the integration of multiple sensing data associated with the same physical process for more comprehensive process representation, thereby improving measurement accuracy and avoid unnecessary sensor cost. A quantification method of data correlation based principle component analysis among sensor measurements in distributed fusion settings or centralized fusion settings was introduced. Orthogonality analysis using the established quantified correlation methodology was performed on the process measurements from four different CSs distributed in the mould cavity as well as MVS installed in the midpoint of cavity. The results show that high correlation exists between measurements from runner pressure sensor and gate pressure sensor and low correlations occur among the measurements of MVS, thus providing an explanation on why a MVS consistently outperformed multiple single-parameter sensors, under various operation conditions.

CHAPTER 7

CONCLUSIONS AND FUTURE WORK

7.1 Conclusions

The goal of this research was to develop a new instrumentation to provide online measurements of four key states critical to the injection molded product quality and wirelessly transmitting the multiple measured parameters through the metal closure using acoustic wave. A new control methodology based on the proposed instrumentation was established for online product quality monitoring.

Specifically, a wireless, embedded multivariate sensing system has been designed, analyzed, prototyped and experimentally evaluated. By taking the mechatronic design approach, the embedded sensing system meets the design criteria and has demonstrated good performance for providing accurate measurements of melt temperature, mold temperature, and melt pressure. Secondly, experimental evaluation on the estimation models for melt velocity and melt viscosity using multivariate sensor (MVS) data was investigated, showing a good correlation with results from sensor-to-sensor model and cross WLF model respectively, thus validating the functionality and performance of MVS. Thirdly, an acoustic-based wireless signal transmission technique was proposed. Signal attenuation and data loss due to wave diffraction and refection was theoretically and experimentally studied on the models of representative machine structures: rectangular and angled structures, where the effect of carrier wav frequency and placement of receiver and transmitter was also investigated experimentally. Lastly, online quality monitoring through in-process measurements from multi-sensor data was then devised based on data fusion algorithm, support vector regression. Outperformance form MVS predication compared with multiple commercial sensor prediction was experimental evaluated.

7.2 Intellectual Contributions

This research has made fundamental contributions to the science and engineering in process measurements and quality control for injection molding and beyond. Major intellectual merits are summarized below.

1) A wireless multivariate sensing system was designed, characterized, and prototyped for in-process quantification of four parameters critical to product quality: melt pressure, temperature, velocity & viscosity, thus providing a new processing instrumentation for improved observability of injection molding.
2) A new acoustic-based wireless signal transmission technique was developed for solving electromagnetic wave shielding in an injection molding machine. This also opens up possibility of data transmission through RF-shielding environments in various manufacturing processes.
3) A data fusion algorithm based on support vector regression model for Injection molding machine was established through in-process measurements using MVS, thus providing a new control methodology that sets up, assures, and optimizes the molded products. In a broader sense, by estimating intrinsic material properties from multiple sensor streams, application-specific process quality models can be developed with high fidelity to guide process control.
4) The developed remote multivariate sensing methodology provides improved observability of process monitoring and adaptive controllability of injection molded product quality, which is the key to automated systems for fault diagnosis, quality control, and materials handling.
5) The framework of orthogonality analysis based on principle component analysis is introduced for quantification of sensor data correlation among multiple measurements, thereby contributing to the theory of data fusion for measurement enhacement.

7.3 Future Work

The established multivariate sensor provides improved observability of polymer processing. An on-line model development and quality control methodology can be developed based on the new process

instrumentation for manufacturers in the process industries with the goal of enabling automated quality assurance. This methodology starts with the characterization of statistical variation for the process while operating in steady state. Significant process conditions are then perturbed by six standard deviations to bound the expected long-term process variation. The designed model-based methodology for online quality control can be used accept and reject manufactured parts given real-time process data, with the capability of detecting of different process faults, such as coolant temperature control off, or barrel temperature adrift +20 ℃ or low cushion. Different algorithm candidates, such as factor analysis, kernel PCA, will be investigated during the system modelling.

In order to provide higher fidelity velocity and viscosity estimation, fast response of infrared temperature sensor is needed to capture the high speed rising front during the melt temperature measurements. Also to provide a much more wide work range for pressure measurement, high yield stress and wide wavelength for the sensor lens is desired for the improvement of multivariate sensor. On-chip scale measuring system with low power consumption, minimized package, and high-signal-to-noise ratio will improve a lot on the current multivariate sensor both in precision and reliability.

As enormous demand on precision of in-process measurements arises, optical sensor, for example, using fluorescence light, for measuring multiple key parameters during polymer processing is highly desired for its successful implementation in chemistry, biology, clinical biology and environmental science. The classical design of a fluorescent indicator includes two moieties, a receptor responsible for the molecular recognition of the analyte and a fluorophore responsible of signaling the recognition event. The fluorescence sensing can provide the measurements of polymeric particles with size ranging from nanometers to micrometers based on dye molecule solutions. Additionally an advantage of fluorescence spectroscopy is that different assays can be designed based on different aspects of the fluorescence output, thus improving the design feasibility during multivariate sensing. Fluorescence techniques are envisioned as the most important future detection method used in the next generation of multivariate sensor.

BIBLIOGRAPHY

[1] Z. Tadmor and C. G. Gogos, Principles of polymer processing, Hoboken, NJ: Wiley-Interscience, 2006.

[2] C. Y. W. Ma, "A Design Approach to a Computer-Controlled Injection-Molding Machine," *Polymer Engineering and Science*, vol. 11, pp. 768-772, 1974.

[3] A. R. Agrawal, I. O. Pandelidis, and M. Pecht, "Injection-Molding Process Control - a Review," *Polymer Engineering and Science*, vol. 27, pp. 1345-1357, 1987.

[4] J. Giboz, T. Copponnex, and P. Mele, "Microinjection Molding of Thermoplastic Polymers: a Review," *Journal of Micromechanics and Microengineering*, vol. 17, pp. 96, 2007.

[5] R. Dubay, A. C. Bell, and Y. P. Gupta, "Control of Plastic Melt Temperature: A Multiple Input Multiple Output Model Predictive Approach," *Polymer Engineering and Science*, vol. 37, pp. 1550-1563, 1997.

[6] D. O. Kazmer, "Precision Process Control of Precision Injection Molding," in *Precision Injection Molding: Process, Materials, and Applications, J. Greener and R. Wimberger-Friedl, Eds. Munich: Carl Hanser Verlag*, 2006, pp. 265-297.

[7] A. Y. Malkin and A. I. Isayev, *Rheology: Concepts, Methods, and Applications*, Chem Tec Publishing 2005.

[8] J. Dininger, "Three Critical Measurements on Injection Molding Processes," *in IEEE Industry Applications Society Annual Meeting*, 1994, pp.2159-2164.

[9] D. O. Kazmer, Plastics Manufacturing Systems Engineering Munich: Carl Hanser Verlag, 2009.

[10] I. A. Rawabdeh and P. F. Petersen, "In-Line Monitoring of Injection Molding Operations: A Literature Review," *Injection Molding Technology*, vol. 3, pp. 47-53, 1999.

[11] K. K. Wang and J. Zhou, "Concurrent-Engineering Approach Toward the Online Adaptive Control of Injection Mdoling Process," *CIRP Annals – Manufacturing Technology*, vol. 49, pp. 379-382, 2000.

[12] C. L. Thomas, A. A. Tseng, A. J. Bur, and J. L. Rose, "Solidification Sensing for Closed Loop Control of Injection Molding Hold Time," *Advances in Polymer Technology*, vol. 15, pp. 151-163, 1996.

[13] P. D. Coates and R. G. Speight, "Toward Intelligent Process Control of Injection Moulding of Polymers," *Proceedings of the Institution of Mechanical Engineers, Part B: Journal of Engineering Manufacture*, vol. 209, pp.357-367, 1995.

[14] D. O. Kazmer, "Precision Process Control," in Precision Injection Molding, J. Greener, Ed.: Hanser, 2004.

[15] A. E. Varela, "Self-tuning Pressure Control in an Injection Moulding Cavity During Filling," *Institute of Chemical Engineers, Part A: Chemical Engineering Research and Design*, vol. 78, pp. 79-86, 2000.

[16] D. H. Muller and Y. Feng, "Reducing Mould-Gap Widths: Avoiding Flash in the Parting Plane of Injection Moulding Machines," *Kunststoffe Plast Europe*, vol. 86, pp. 7-9, 1996.

[17] O. Vaatainen, P. Jarvela, and K. Valta, "The Effect of Processing Parameters on the Quality of Injection Moulded Parts," *Plastics, Rubber, and Composites Processing and Applications*, vol. 21, pp. 211, 1994.

[18] J. Oehlmann, "Intelligent camera," *Kunststoffe Plast Europe*, vol. 89, pp. 21-22, 1999.

[19] J. Agassant, P. Avanas, J. Sergent, and J. Garreau, Polymer Processing: Principles and Modeling, New York: Hanser Publishers, 1991.

[20] T. Aeppel, "Workers Not Included," in *The Wall Street Journal New York*, 2002.

[21] R. Collins, G. Cranny, J. Burch, R. Aguiar-Ibáñez, D. Craig, K. Wright, E. Berry, M. Gough, J. Kleijnen, and M. Westwood, "A Systematic Review of Duplex Ultrasound, Magnetic Resonance Angiography and Computed Tomography Angiography for the Diagnosis and Assessment of Symptomatic, Lower Limb Peripheral Arterial Disease," *Health technology assessment (Winchester, England)*, vol. 11, 2007.

[22] M. Savelonas, D. Iakovidis, I. Legakis, and D. Maroulis, "Active Contours Guided by Echogenicity and Texture for Delineation of Thyroid Nodules in Ultrasound Images," *IEEE Transactions on Information Technology in Biomedicine*, vol.13, no.4, pp.519-527, 2009.

[23] D. Zhang, M. Donovan, L. L. Fajardo, A. Archer, X. Wu, and H. Liu, "Preliminary Feasibility Study of an In-line Phase Contrast X-Ray Imaging Prototype," *IEEE Transactions on Biomedical Engineering*, vol.55, no.9, pp.2249-2257, 2008.

[24] W. Michaeli and C. Starke, "Ultrasonic Investigations of the Thermoplastics Injection Moulding Process," *Polymer Testing*, vol. 24, pp. 205-209, 2005.

[25] B. He, X. Zhang, Q. Zhang, and Q. Fu, "Real-time Ultrasonic Monitoring of the Injection-Molding Process," *Journal of Applied Polymer Science*, vol. 107, 2008.

[26] C. B. Theurer, L. Zhang, D. O. Kazmer, R. X. Gao, and R. W. Jackson, "A Self-Energized Sensor for Wireless Injection Mold Cavity Pressure Measurement: Design and evaluation," *IEEE Sensors Journal*, vol. 6, pp. 47-54, 2006.

[27] L. Zhang, C. B. Theurer, R. X. Gao, and D. O. Kazmer, "Design of Ultrasonic Transmitters with Defined Frequency Characteristics for Wireless Pressure Sensing in Injection Molding," *Journal of Dynamic Systems, Measurement, and Control*, vol. 126, pp. 309-318, 2004.

[28] L. Zhang, C. B. Theurer, R. X. Gao, and D. O. Kazmer, "Design of Ultrasonic Transmitters with Defined Frequency Characteristics for Wireless Pressure Sensing in Injection Molding," *IEEE Transactions on Ultrasonics, Ferroelectrics and Frequency Control*, vol. 52, pp. 1360-1371, 2005.

[29] R. X. Gao, Z. Fan, and D. O. Kazmer, "Design of an Acoustic Transmitter for Temperature-Pressure Dual Sensing in Injection Molding, " *Proceedings of 2006 IEEE Sensors Conference, Paper No.1478, Daegu, Korea*, 2006.

[30] R. X. Gao, Z. Fan, and D. O. Kazmer, "Injection Molding Process Monitoring Using a Self-Energized Dual Parameter Sensor," *CIRP Annals - Manufacturing Technology*, vol.57, pp.389-393, 2008.

[31] Z. Fan, R. X. Gao, and D. O. Kazmer, "Design and Evaluation of a Modulator Circuit for a Self-Energized Wireless Sensor," *Proceedings of ASME International Mechanical Engineering Congress and Exposition, Paper No.67848, Boston, MA*, 2008.

[32] U. Langkamp, "Pressure and temperature sensors," *Kunststoffe Plast Europe*, vol. 86, pp. 1804-1812 German, 1996.

[33] J. W. Mann, "Process Parameter Control: the Key to Optimization," *Plastics Engineering*, vol. 30, pp. 25-27, 1974.

[34] M. R. Kamal, W. I. Patterson, N. Conley, D. Abu Fara, and G. Lohfink, "Dynamics and Control of Pressure in the Injection Molding of Thermoplastics," *Polymer Engineering and Science*, vol. 27, pp. 1403-1410, 1987.

[35] K. Srinivasan and T. Brinivasan, "Learning Control of Melt Pressure in Injection Molding Processes," in *American Society of Mechanical Engineers, Dynamic Systems and Control Division (Publication) DSC*, Atlanta, GA, USA, 1991, pp. 151-159.

[36] F. Gao, I. A. N. Patterson, and M. R. Kamal, "Self-Tuning Cavity Pressure Control of Injection Molding Filling," *Advances in Polymer Technology*, vol. 13, pp. 111-120, 1994.

[37] D. O. Kazmer and P. Barkan, "Process Capability of Multi-Cavity Pressure Control for the Injection Molding Process," *Polymer Engineering and Science*, vol. 37, pp. 1880-1895, 1997.

[38] M. Moss, "Controlling the Injection Molding Process," in *The Plastics America Agenda: Structured Plastics Institute*, 1999, pp. 111-113.

[39] D. O. Kazmer, D. Gupta, M. Munavalli, V. Kudchadkar, and R. Nageri, "Design and Performance Analysis of a Self-Regulating Melt Pressure Valve," *Polymer Engineering and Science*, vol. 46, pp. 549-557, 2006.

[40] D. O. Kazmer and D. Gupta, "A low Force Valve for Dynamic Control of Molten Plastics in a Mold," *International Polymer Processing*, vol. 21, pp. 175-182, 2005.

[41] Z. Chen and L. S. Turng, "Injection Molding Quality Control by Integrating Weight Feedback into a Cascade Closed-loop Control System," *Polymer Engineering & Science*, vol. 47, 2007.

[42] D. O. Kazmer, S. Westerdale, and D. Hazen, "A Comparison of Statistical Process Control (SPC) and On-Line Multivariate Analyses (MVA) for Injection Molding," *International Polymer Processing*, vol. 23, pp. 447-458, 2008.

[43] S. Johnston and D. O. Kazmer, "Decoupled Gating and Simulation for Injection Molding," *Polymer-Plastics Technology and Engineering*, vol. 45, pp. 575-584, 2006.

[44] D. O. Kazmer, R. Nageri, V. Kudchakar, B. Fan, and R. X. Gao, "Validation of Three On-Line Flow Simulations for Injection Molding," *Polymer Engineering and Science*, vol. 46, pp. 274-288, 2006.

[45] D. O. Kazmer, P. Knepper, and S. Johnston, "A Review of in-Mold Pressure and Temperature Instrumentation," *in SPE Annual Technical Conference, Process Monitoring & Control Group, Boston, MA, United States*, 2005, pp. 375-379.

[46] C. B. Theurer, L. Zhang, D. O. Kazmer, and R. X. Gao, "Energy Extraction for a Self-Energized Pressure Sensor," *IEEE Sensors Journal*, vol. 4, pp. 28-35, 2004.

[47] C. B. Theurer, L. Zhang, D. O. Kazmer, R. X. Gao, and R. W. Jackson, " A Self-Energized Sensor for Wireless Injection Mold Cavity Pressure Measurement: Design and evaluation," *IEEE Sensors Journal*, vol. 6, pp. 47-54, 2006.

[48] H. C. Hottel and A. F. Sarofim, Radiative Transfer: McGraw-Hill Education, 1967.

[49] J. Bicerano, Prediction of polymer properties: CRC, 2002.

[50] K. Ulrich and S. Eppinger, Product design and development. McGraw-Hill, 2004.

[51] Chang, R.Y. and Tsaur, B.D., "Experimental and theoretical studies of shrinkage, warpage, and sink marks of crystalline polymer injection molded parts, " *Polymer Engineering and Science*, vol. 35, no. 15, pp. 1222-1230, 1995.

[52] Chao, A. and Chen, R., 2008, "The experimental study on the defects occurrence of SL mold in injection molding," *Materials Processing Technology*, vol. 201, no.1-3, pp. 706-709, 2008.

[53] Orzechoweski, S., Paris, A., and Dobbin, C., "A process and control system for injection molding using nozzle-based pressure and temperature sensors, " *Proceedings of ANTEC 1998 Plastics, Atlanta, GA*, vol. 1, pp. 424-430, 1998.

[54] Tie G., Dequn, L., and Huamin, Z., 2006, "Three dimensional finite element method for the filling simulation of injection molding," *Engineering with Computers 21*, pp. 289-295, 2006.

[55] Yang, Y. and Furong, G., "Injection velocity control based on an iterative learning and feedback combined controller, " *8th International Symposium on Advanced Control of Chemical Processes*, *Gramado, Brazil*, vol. 1, pp. 385-390, 2006.

[56] Gao, R. X., Fan, Z., and Kazmer, D. O., "Injection molding process monitoring using a self-energized dualparameter sensor," *CIRP Annals – Manufacturing Technology*, vol. 57, pp. 389-393, 2008.

[57] Ono, Y., Jen, C. K., Cheng, C. C., and Kobayashi, M., "Real-time monitoring of injection molding for microfluidic devices using ultrasound," *Polymer Engineering & Science*, vol. 45, no. 4, pp. 606–612, 2005.

[58] Suh, W. J., and Lee, Z. H., "Melt velocity measurement by a no contacting electromagnetic probe," *Review of Scientific Instruments*, vol. 71, no.5, pp. 2241-2245, 2000.

[59] Whatmore, R. W., "Pyroelectic devices and materials," *Reports on Progress in Physics*, vol. 49, no. 12, pp. 1335-1386, 1986.

[60] Maier, C., "infrared temperature measurement of polymers," *Polymer Engineering and Science*, vol. 36, no. 11, pp. 1502-1512, 1996.

[61] Porter, S.G., "A brief guide to pyroelectric detectors," *Ferroelectronics*, vol.33, no.1, pp. 193-206, 1986.

[62] Johnston, S., Kazmer, D. O., and Gao, R. X., "In-Mold temperature and pressure sensors for on-line detection of jetting," *Proceedings of ANTEC 2008 Plastics, Milwaukee, WI*, 2008, vol. 54, pp. 2376-2380.

[63] G. Gordon, D. O. Kazmer, R. X. Gao, Z. Fan, and N. A. Zanjani, "Temperature Modeling for a Multivariate Injection Molding Sensor," *presented at the Society of Plastics Engineers (SPE) ANTEC, Cincinnati, OH*, 2013.

[64] Binxin, Y., Jie, O., Chuntai, L., and Qiang, L., "Simulation of non-isothermal injection molding for a non-Newtonian fluid by level set method," *Chinese journal of chemical engineering*, vol. 18. no. 4, pp.600-608, 2010.

[65] Reference for Cross WLF model

[66] Abbate A, Koay J, Frankel J, Schroeder SC, Das P, "Signal Detection and Noise Suppression Using Wavelet Transformation Signal Processor: Application to Ultrasonic Flaw Detection," *IEEE Transactions on Ultrasonics Ferroelectrics and Frequency Control*, vol. 44, no. 1, pp. 14–26, 1997.

[67] Kim G, Yoon C, Kye S, Lee Y, Kangs J, Yoo Y, Song T, "A Single FPGA-Based Portable Acoustic Imaging System for Point of Care Applications," *IEEE Transactions on Ultrasonics Ferroelectrics and Frequency Control*, vol. 59, no. 7, pp.1386–1394, 2012.

[68] Bramanti M, "A Nondestructive Method on Swept Frequency Acoustic Transmission Reflection Measurements," *IEEE Transactions on Instrumentation and Measurement*, vol. 41, no. 4, pp.490–494, 1992.

[69] Stoebener D, Dijkman M, "An Acoustic In-Process-Measuring System to Ensure a Minimum Roundness Deviation for Rings During Turning," *CIRP Annals– Manufacturing Technology*, vol. 56, no. 1, pp.513–516, 2007.

[70] Shinno H, Hashizume H, Sato H, "In-Process Monitoring Method for Machining Environment Based on Simultaneous Multiphenomena Sensing," *CIRP Annals– Manufacturing Technology*, vol. 46, no. 1, pp.53–56, 1997.

[71] Gao R, D.O. Kazmer, "Multivariate Sensing and Wireless Communication for Process Monitoring in RF-Shielded Environment," *CIRP Annals – Manufacturing Technology*, vol. 61, no. 1, pp.523–527, 2012.

[72] Beitz W, Kuttner KH, Davis BJ, Handbook of Mechanical Engineering, Springer-Verlag, New York, 1994.

[73] Kinsler LE, Frey AR, Coppens AB, Sanders JV, Fundamentals of Acoustics, John Wiley & Sons, New York, NY, 1999.

[74] Wirtz A., Gachter C., Wipf D., "From unambiguously defined geometry to the perfect quality control loop," *CIRP Annals – Manufacturing Technology*, vol. 42, no.1, pp.615-618, 1993.

[75] Hashimoto F., Guo Y., Warren A., "Surface integrity difference between hard turned and ground surfaces and its impact on fatigue life," *CIRP Annals*, vol. 55, no. 1, pp. 81-84, 1994.

[76] Kakinuma Y., Sudo Y., Aoyama T., "Detection of chatter vibration in end milling applying disturbance observer," *CIRP Annals*, vol. 60, no. 1, pp.109-112, 2011.

[77] Teti R., Jemielniak K., O'Donnell G., Dornfeld D., "Advanced monitoring of machining operations," *CIRP Annals*, vol. 59, no. 2, pp.717-739, 2010.

[78] Cloizeaux, J., "Relaxation and viscosity anomaly of melts made of long entangled polymers," *Macromolecules*, vol. 23, no. 1, pp.4678-4687, 1990.

[79] Fischer J., "Controlling Mold and Postmold Shrinkage and Warpage," in *Handbook of Molded Part Shrinkage and Warpage, ed Oxford*, UK: William Andrew Publishers, 2013.

[80] Liu C., Manzione L., "Process studies in precision injection moulding: process parameters and precision," *Polymer Engineering & Science*, vol. 36, no. 1, pp.1-9, 1996.

[81] Kazmer D., Westerdale S., "A model-based methodology for on-line quality control," *Int. J. Adv. Manuf. Technol.*, vol. 42, no. 1, pp.280-292, 2009.

[82] T. Hastie, R. Tibshirani, and J. Friedman, The Elements of Statistical Learning. Springer, 2009.

[83] V. Vapnik, Statistical Learning Theory. New York: Wiley, 1998.

[84] Kazmer D., Johnston S., Gao R., Fan Z., "Feasibility analysis of an in-mold multivariate sensor," *International Polymer Processing*, vol. 26, no. 1, pp.63-72, 2011.

[85] Chang R., Chen C., Su K., "Modifying the Tait equation with cooling-rate effects to predict the volumetric shrinkage," *Polymer Engr. and Sci*., pp.1789-1795, 1996.

[86] C.Y. Chong, S. Mori, K.C. Chang, and W.H. Barker, "Architecture and algorithms for track association and fusion," *IEEE Aerospace and Electronic Systems*, vol. 15, no. 1, pp. 5-13, Jan. 2000.

[87] E. Waltz and J. Llinas, Multisensor Data Fusion, Artech House, 1990.

[88] R.C. Luo, C.C. Chang, and C.C. Lai, "Multisensor fusion and integration: theories, application, and its perspectives," *IEEE Sensors Journal*, vol. 11, no. 12. Dec. 2011

[89] I. T. Jolliffe, Principal Component Analysis, *second edition*, Springer, 2002.